Answer to:

Interactive comment on "Impact of the South Asian monsoon outflow on atmospheric hydroperoxides in the upper troposphere" by Bettina Hottmann et al.

Anonymous Referee #1.

(black: RC, red: AC, blue: changed in manuscript)

This study presents observations of hydroperoxides during an aircraft campaign investigating the outflow of the south Asian summer monsoon and how it affects the composition of the Asian Monsoon Anticyclone (AMA). The observations of H2O2 and ROOH are enhanced in the AMA, which the authors suggest is due to convective transport of these species. The authors compare these observations to steady state calculations constrained by observed OH, HO2, and photolysis frequencies as well as to the results of the EMAC global model. I have three major concerns regarding this study, which I summarize below, followed by more minor comments.

Major concerns:

1) The inferred UHP is taken as the difference between measured ROOH and PSS MHP. The basis for this is not clear to me, as it assumes that MHP is accurately simulated by the PSS calculations. Given that the PSS H2O2 calculation underestimates observed H2O2 by a significant amount (up to a factor of 10!), there is no reason to believe that the PSS MHP doesn't suffer from the same problem. I found the use of UHP to be very confusing as it sometimes referred to as PSS UHP or calculated UHP or observed UHP. Given that what is measured is H2O2 and ROOH, I suggest that the authors only use these two quantities throughout the manuscript and compare them to PSS H2O2, PSS MHP, EMAC H2O2, EMAC ROOH, thus removing any use of UHP.

We are sorry for the confusion. As mentioned in the experimental section, the ROOH measurement is unspecific and due to the different solubilities of hydroperoxides only qualitative. In order to estimate the amount of MHP, which according to previous measurements is expected to be the dominant (if not the only) ROOH component, we calculated the amounts of MHP from a photo-stationary state calculation (as well as H2O2). The difference between ROOH and PSS MHP is unexplained or unaccounted for, thus we named it UHP. As discussed in the paper UHP can be due to an unidentified hydroperoxide (e.g. PAA), additional MHP due to advection or a combination of both. Since no specific ROOH measurements were made nor does the 3D-model indicate substantial amount of hydroperoxides other than MHP, we cannot finally decide on the nature (or composition) of the UHP. In the revised manuscript, we will more clearly define UHP and follow the referee in using PSS H2O2, PSS MHP, EMAC H2O2, EMAC ROOH in addition to EMAC MHP. Nevertheless we would still like to use UHP in the sense of an unaccounted for hydroperoxide either as additional MHP (exceeding PSS MHP) and/or a significant contribution by an organic hydroperoxide not simulated in EMAC (e.g. PAA).

Section 4.3.2 changed to:

Figure 14 shows histograms for the comparison between H2O2, MHP and UHP observations with EMAC simulations. Hydrogen peroxide simulations from EMAC cover a broader range of mixing ratios for both NH background (6 pptv up to 576 pptv) and AMA (8–714 pptv) compared to observations (NH background: 20–301 pptv; AMA 46–446 pptv). For the SH model simulations and observations indicate almost identical ranges of 15–409 pptv and 85–510 pptv, respectively. Median EMAC-H2O2 values are similar for NH background (66 pptv) and AMA (71 pptv) conditions (Table 2), while observations indicate an enhancement of +64 pptv in the AMA relative to the NH background. For the SH the model simulated H2O2 mixing ratios are four times higher than in the NH background (272 pptv), while the observations only show a median increase by 47 pptv to 211 pptv (Table 2).

EMAC mainly simulates MHP mixing ratios lower than 50 pptv for background and AMA, while PSS-MHP ranges from LOD–140 pptv. Again the model simulates highest MHP mixing ratios in the SH with values up to 502 pptv compared to up to 346 pptv in the PSS-MHP calculations. Similar as for H2O2, medians of EMAC-MHP for NH background and monsoon conditions are almost identical (11 pptv and 13 pptv respectively, Table 2) in the model simulations, while the observations show a small difference towards higher mixing ratios in the AMA (64 pptv and 70 pptv, respectively). In the simulations, southern hemispheric EMAC-MHP mixing ratios are almost ten times higher than NH background values, compared to two to three times higher ones in the observations.

Data for UHP in the model are calculated from the sum of simulated ethyl hydroperoxide (EHP) and peroxyacetic acid (PAA), which are the only non-methyl organic hydroperoxides in the free troposphere according to the model. EMAC-UHP mixing ratios range from 1–238 pptv in the NH background, 1–259 pptv in the AMA and 1–132 pptv in the SH. PSS-UHP based on the observations indicate lowest mixing ratios in the NH background (LOD–261 pptv), while in the AMA and the SH the ranges are quite similar (80–311 pptv and LOD–334 pptv). A comparison of median values emphasizes the large difference between model simulations and observation-based estimates. In the NH background, the median PSS-UHP mixing ratio from the observations is 70 pptv higher than EMAC simulations (78 pptv and 8 pptv respectively). In the AMA the difference is even larger, with about 200 pptv higher PSS-UHP levels compared to the EMAC simulations. The smallest difference with a factor of four was found for the SH (Table 2).

2) Throughout the manuscript (including the abstract and conclusions) the comparisons between observations and model results (both PSS and EMAC) are described in very vague and qualitative terms (such as "observed concentrations are higher than model calculations", "the model underestimates H2O2", etc. . .). This lacks rigor and leaves the reader unsure about the magnitude of the misrepresentation of the models. I strongly encourage the authors to be more quantitative in their comparisons throughout the manuscript, using statistical measures, which could include mean bias, normalized mean bias, FAC2, RMSE, etc. . . The figures and tables should include these statistical measures.

We added the ranges, averages and standard deviations for the in-situ and PSS comparison (Table 1). In addition we added more statistical information in table 2 (former table 1). The abstract as well as conclusion were changed so that they are more quantitative.

Abstract changed to:

L22: We observed enhanced mixing ratios of H2O2 (45%), MHP (9%) and UHP (136%) in the AMA relative to the northern hemispheric background. Highest concentrations for H2O2 and MHP of 211 ppbv and 152 ppbv, respectively were found in the tropics outside the AMA, while for UHP, with 208 pptv, highest concentrations were found within the AMA. In general, the observed concentrations are higher than steady-state calculations and EMAC simulations. Especially in the AMA, EMAC underestimates the H2O2 (medians: 71 pptv vs. 164 pptv) and ROOH (medians: 25 pptv vs. 278 pptv) mixing ratios.

Conclusion changed to:

L471: The atmospheric chemistry-general circulation model EMAC slightly underestimates H2O2 in the NH background (medians: 66 pptv vs. 100 pptv), but significantly underestimates it in the AMA (medians: 71 pptv vs. 164 pptv), and overestimates it in the SH (medians: 272 pptv vs. 211 pptv). Steady-state calculations for H2O2 and MHP based on observed precursors yield much lower values, in particular in the AMA, resulting in a large contribution of an unidentified organic hydroperoxide (UHP) in air masses affected by the Asian summer monsoon.

New table added:

Table 1: Comparison of H_2O_2 mixing ratios in the upper troposphere from measurements and PSS calculations.

region	median	$[H_2O_2]/ppt_v$
PSS	median range avg±sdev	15 LOD–657 61±101
HYPHOP	median range avg±sdev	150 LOD–530 165±91

And thus former Table 1 Is now Table 2.

Section 4.3.1 starting with line 357 changed to:

The regression coefficient is quite high (0.83), even though most of the calculated steady-state mixing ratios (75%) are in the range between 0 and 65 pptv with a median value of 15 pptv, while the measured mixing ratios extend over a larger range mainly between 10–210 pptv with a median of 150 pptv and thus 10 times higher than for steady-state, which can also be seen in the histograms in Figure 13. Table 1 shows the statistical comparison of both data sets.

Table 2 changed to:

Table 2: Comparison of H_2O_2, MHP and UHP mixing ratios in the upper troposphere from EMAC, measurements and PSS calculations.

region	median	$[H_2O_2]/ppt_v$		$[MHP]/ppt_v$		$[UHP]/ppt_v$	
		EMAC	HYPHOP	EMAC	PSS	EMAC	PSS

NH background	median range avg±sdev	66 6–576 102±110	100 20–301 110±53	11 2–408 28±58	64 21–202 75±42	8 1–238 18±31	78 LOD–261 103±77
monsoon	median range avg±sdev	71 8–714 84±92	164 46–446 167±69	13 2–216 18±28	70 37–220 92±49	12 1–259 18±34	208 80–311 199±59
SH background	median range avg±sdev	272 15–409 272±68	211 85–510 238±105	116 2–502 155±125	152 40–346 191±95	33 1–132 42±24	122 LOD–334 125±102

Title of Fig. 13 changed to: "Figure 13: Histograms of measured (top) and calculated (bottom) H2O2 mixing ratios (bars) and the associated medians (lines)."

3) The authors suggest that deviation between EMAC and observed H2O2 and ROOH are due to uncertainties in the scavenging efficiencies of these species in the model. As described in line 430 "..sensitivity study with EMAC excluding scavenging". This sentence seems to suggest that scavenging of all species is turned off, which seems like a rather brute force method as lack of scavenging of other species could in turn affect the photochemical evolution of H2O2 and ROOH. A simulation in which scavenging of only H2O2 and ROOH is turned off seems more appropriate. Also, is scavenging turned off only for the AMA region or the entire globe? If it is for the entire globe, then the difference between the simulations might not be related to processes associated with convection over India. It seems that the link between convection and peroxides could be investigated more carefully with EMAC, including a more targeted sensitivity simulation, and also examining correlations of modeled peroxides and NO/NOy ratio as well as acetone. Also, the authors do not discuss how well convection is represented in the model in the first place. For example how well does EMAC reproduce observations of species that are not scavenged (such as CO or some VOCs)?

- CO in the upper troposphere is lower in EMAC due to weaker convective transport (possibly caused by the low resolution of the global model) as described in Tost et al. (2016) and Tomsche et al. (2019).

Tost, H., Jöckel, P., and Lelieveld, J.: Influence of different convection parameterisations in a GCM, Atmos. Chem. Phys., 6, 5475–5493, https://doi.org/10.5194/acp-6-5475-2006, 2006

-As described in Klippel et al., scavenging of all soluble species was turned off in the model, not only for the Indian sub-continent. Since the purpose of the sensitivity study is to calculate the maximum amount of H2O2 that can be transported into the AMA, we believe that this is justified. Simultaneous wash-out of other soluble species (HNO3, organic acids etc) will not directly affect H2O2 but might change HOx levels, thus affect H2O2 through secondary chemistry. Also convective addition of H2O2 in other regions (e.g. the West African Monsoon) will hardly affect H2O2 levels in the AMA due to the limited lifetime of H2O2.

Minor Comments

Sections 3.3, 3.4: Can the authors indicate the lifetimes of H2O2 and MHP during flight conditions? This will be useful to assess the validity of the PSS assumption. In particular, the validity of PSS will also depend on time of day/SZA. For what conditions do the authors apply PSS?

The lifetime of H_2O_2 is around 4 days and MHP around 1 day. Major losses are the reaction with OH and photolysis by sunlight. No special conditions were applied to the calculations as the aim was to estimate local photochemistry. Measurements were only performed during daytime.

Line 258. The authors mention that the data were averaged in 60 second intervals. It wasn't clear from the description what the frequency of the measurements were, in particular for H2O2, ROOH and the species used to calculate PSS.

Data are from merged data sets which were calculated from the original data that were recorded with a higher resolution. For H_2O_2 and ROOH we record 1 value per second, TRISTAR (CH_4 and CO) appr. 1 per second, OH and HO_2 appr. 4 per minute, NO and NO_y 1 per second, J values 1 value per 1 or 2 seconds.

Changed to:

L272: Data were collected from a merged data set given as 60-second-means (calculated from the original data set obtained at higher resolutions) in order to get the same time resolution for all compounds.

Figure 2. Can the authors indicate the number of days for which the back trajectories were calculated?

Ten day back trajectories were used.

The title of the figure is changed to:

Figure 2: Track of flight 17 (black dotted line) and calculated 10-day-back trajectories (lines colored as a function of altitude) to show the origin of sampled air masses during the flight.

Figures 3. It is unclear why the authors show the data on the timescale of the EMAC model, given that in the text (line 263) the authors say that the model was interpolated in time and space along the flight track. Given that the observations are likely available at a higher time resolution as can be seen in Figure 4, it might make more sense to show the observations at their original time resolution instead of the much coarser 10-15 minute resolution of EMAC.

EMAC results are obtained at a temporal resolution of 12 min and spatial resolution of 2.8° x 2.8°, and interpolated in space along the flight track. Therefore, any interpolation to higher time resolution of this dataset would not provide any added value.

Changed to:

L253: For this study EMAC simulations were performed for the OMO flight tracks in 2.8°x2.8° grids with a time resolution of 12 minutes.

Figures 6&7 (as well as Figures 10&11) and lines 295-3050. The authors discuss the correlation of UHP with acetone and NO/NOy, without mentioning the correlation with the other peroxides. First, given that

UHP is inferred based on the PSS calculation, it would make more sense to use observed ROOH. Also, nased on looking at Figure 4, it seems that H2O2 might also be correlated with acetone and NO/NOy. Correlations (or lack thereof) with H2O2 should be discussed in the text.

Following the suggestion, we have provided the requested relations. Please note that a positive correlation not necessarily indicates a relation to a precursor. It can also indicate a co-location of sources.

Section changed to:

L311: The PSS-UHP and acetone mixing ratios in this part of the flight are strongly correlated (Figure 6), with a slope of 0.19±0.02 (ppbv/ppbv) and an offset of (-0.003±0.02) ppbv. The regression coefficient R2 is very high (0.99). For H2O2 and ROOH the correlation is not that strong with slopes of -0.02±0.02 (ppbv/ppbv) and 0.13±0.03 (ppbv/ppbv), respectively, and offsets of (0.21±0.02) ppbv and (0.11±0.03) ppbv (Figure 6). The relation between ROOH mixing ratios and an air mass age tracer based on the ratio between [NO] to [NOy] shows higher values of ROOH at smaller ratios representing older or more processed air masses (Figure 7), since highest ROOH mixing ratios (>200 pptv) are found at the lowest [NO]/[NOy] ratios (all <0.19). Thus, most of the observed ROOH was measured in aged air masses transported within the anticyclone. The correlation with PSS-UHP shows that this effect is mainly due to PSS-UHP. For H2O2 there are also some higher mixing ratios for high [NO] to [NOy] mixing ratios and thus fresher air (Figure 7).

Section changed to:

L344: In the analysis of flight 17 we found a strong correlation between PSS-UHP and acetone (Figure 6) and an increase of PSS-UHP at the oldest air mass ages, represented by low [NO]/[NOy] (Figure 7). Extension of this analysis to all observations in the upper troposphere obtained during OMO yields similar results for the relation between PSS-UHP, in situ ROOH and in situ H2O2 and acetone (Figure 10). Enhanced mixing ratios of hydroperoxides are typically associated with enhanced acetone mixing ratios, especially for PSS-UHP. A simple calculation of the production of MHP out of the photolysis of acetone and the reaction of acetaldehyde (from EMAC) with OH shows that per day appr. 40 pptv MHP can be formed within the AMA. The lifetime of MHP was calculated to be around 1.5 days. Thus not all of the PSS-UHP in the AMA (median 210 pptv) can be accounted for by MHP that was chemically produced from VOCs in the AMA. The scatter plots of the hydroperoxides vs. [NO]/[NOy] for the whole data set, show no clear correlation with a large spread of hydroperoxides mixing ratios at the lowest [NO]/[NOy] ratios, representing the oldest, i.e. chemically most processed air masses (Figure 11).

Figures 6 and 7 changed to:

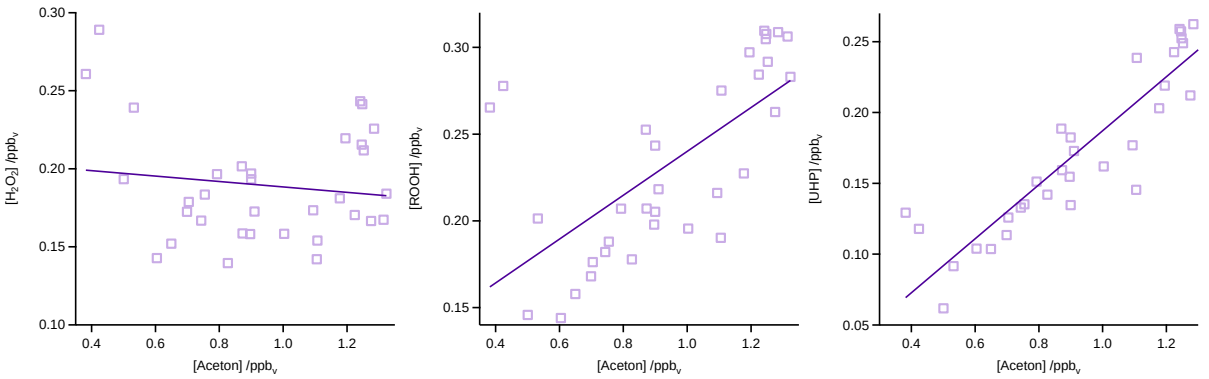

Figure 6: Scatter plots of measured acetone and in situ H2O2 (left), in situ ROOH (middle) and PSS-UHP (right) during flight 17. The black lines represent the least orthogonal distance fits with regression coefficients of 0.99, 0.98 and 0.99.

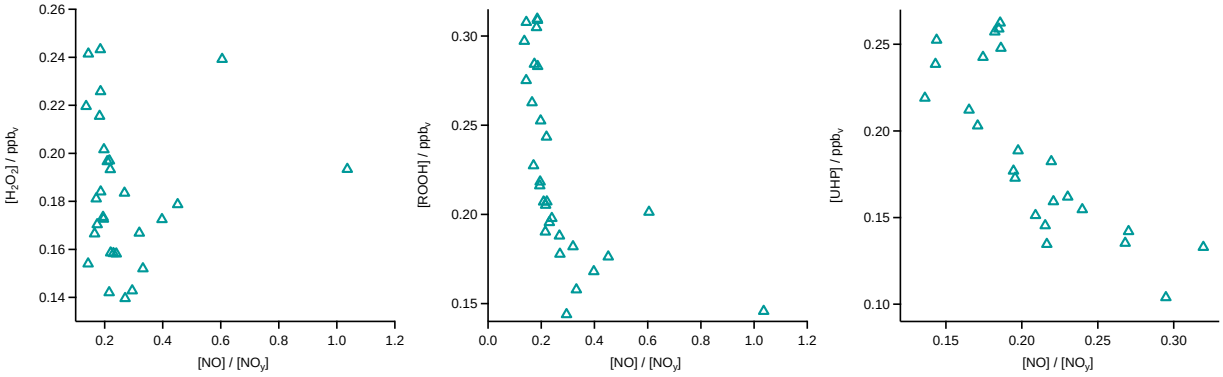

Figure 7: Scatter plots of in situ H2O2 (left), in situ ROOH (middle) and PSS-UHP (right) and NO/NOy ratio during flight 17.

Figures 10 and 11 changed to:

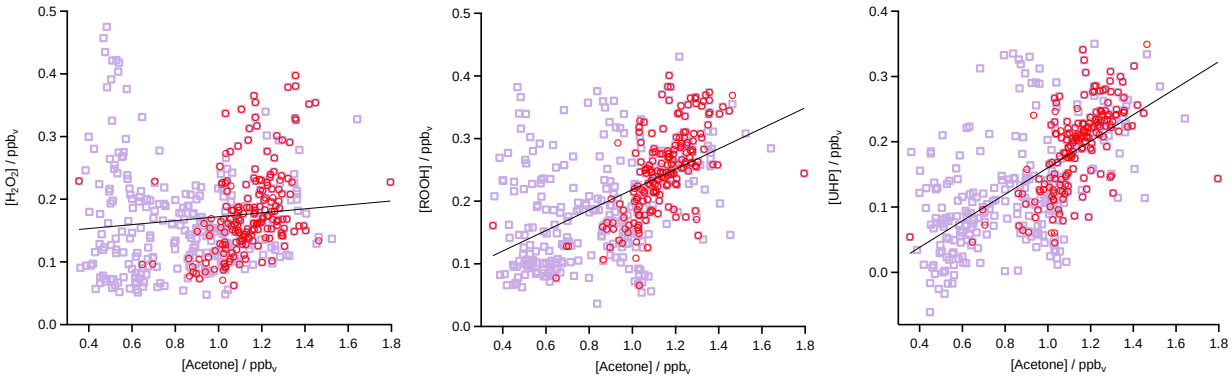

Figure 10: Scatter plots of in situ acetone and in situ H2O2 (left), in situ ROOH (middle) and PSS-UHP (right) in the UT (purple squares) and especially in the AMA (red circles). The black lines represent the least orthogonal distance fit with linear regression coefficients of 0.96 (H2O2), 0.97 (ROOH) and 0.96 (UHP).

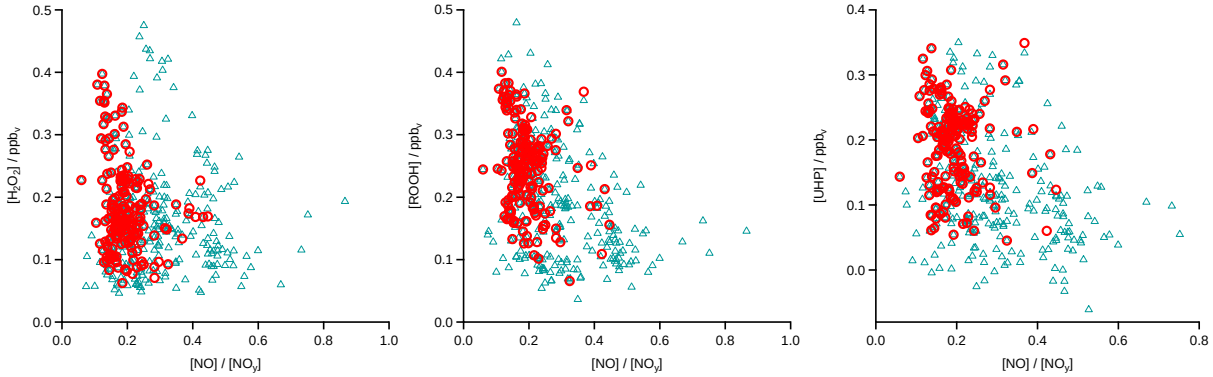

Figure 11: Scatter plots of NO/NOy and in situ H2O2 (left), in situ ROOH (middle) and PSS-UHP (right) in the UT (blue triangles) and especially in the AMA (red circles).

Line 336 "The deviations from unity in the slope are within the combined uncertainties of measured and steady-state estimations of H2O2 (51%, 1 σ)" Looking at Figure 12, it looks like most points are outside the +/- 51% range. Can the authors be more quantitative and state the number of points outside the uncertainties?

82% of points are outside the range of the uncertainties of ± 51%.

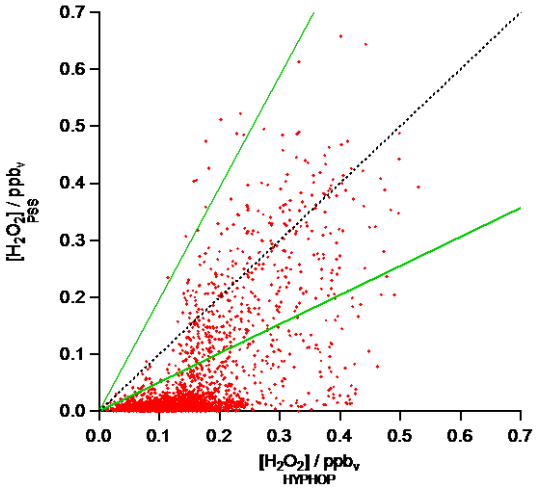

Section 4.3.2 In the comparison to EMAC, the authors tend to focus on the range of modeled and observed values, which is not very informative. It would be more useful to discuss means or medians and provide statistical measures of the model/observations mismatch (such as mean bias, mean normalized bias, mean normalized gross error, etc. . .). Also to put the comparison of EMAC to peroxides in perspective, it would be useful if the authors could discuss the comparisons to other tracers (acetone, O3, H2O, CO, NOx, NOy, aerosols, etc. . .), which might shed light on whether the mismatch is an issue related to emissions, transport, scavenging, or chemistry.

Table 2 was changed (see above). In addition we want to refer to Lelieveld et al., 2018 where a detailed comparison of observed and modelled data is shown.

Line 379. Many other studies before Bozem et al. (2017) have shown the role of deep convection as a source of peroxides in the upper troposphere, including Prather and Jacob (1997), Jaeglé et al. (1997), Mari et al. (2002) among others.

Line 404 (former 379) was changed to

In contrast, other studies found that deep convection can be a source of H2O2 in the upper troposphere (e.g. Jaeglé et al., 1997; Prather and Jacob, 1997; Mari et al., 2003; Bozem et al., 2017).

Lines 386-390. The authors fail to mention the very large underestimate of EMAC ROOH compared to observations.

Here we focus on the qualitative analysis of the longitudinal gradients and thus on the trends along the longitude. Including the additional information, the difference between in situ data and the EMAC model is discussed quite elaborately now.

References:

Jaeglé, L., et al.: Observed OH and HO2 in the upper troposphere suggest a major source from convective injection of peroxides, Geophys. Res. Lett., 24, 3181–3184, https://doi.org/10.1029/97GL03004, 1997. Mari, C., et al., On the relative role of convection, chemistry, and transport over the South Pacific Convergence Zone during PEMâA˘ RTropics B: A case study, J. Geophys. ˘ Res., 107, 8232, doi:10.1029/2001JD001466, 2002. C4 ACPD Interactive comment Printer-friendly version Discussion paper Prather, M. J. and Jacob, D. J.: A persistent imbalance in HOx and NOx photochemistry of the upper troposphere driven by deep convection, Geophys. Res. Lett., 24, 3189– 3192, https://doi.org/10.1029/97GL03027, 1997. Interactive comment on Atmos. Chem. Phys. Discuss., https://doi.org/10.5194/acp-2020-93, 2020.

Answer to: Interactive comment on "Impact of the South Asian monsoon outflow on atmospheric hydroperoxides in the upper troposphere" by Bettina Hottmann et al.
Anonymous Referee #2

Please note the colour code
(black: RC, red: AC, blue: changes in manuscript)

The paper describes aircraft measurements of hydroperoxide compounds and supporting observations taken during the Oxidation Mechanism Observation (OMO) mission. These measurements are analyzed alongside photochemical steady state calculations, trajectory modeling, and global model simulations to understand the source regions of the air sampled in the upper troposphere. The major findings are that hydroperoxide mixing ratios are enhanced in the Asian Monsoon Anticyclone (AMA) compared to the background Northern Hemisphere (NH) mixing ratios, but highest hydrogen peroxide (H2O2) and methyl hydrogen peroxide (CH3OOH) mixing ratios were found in the background Southern Hemisphere (SH). The authors attribute the high mixing ratios in the AMA to upwind convection, using a sensitivity simulation with the global model EMAC to support this claim.
It is interesting to discover the higher-than-expected hydroperoxide mixing ratios in the Asian Monsoon Anticyclone, and then learn what caused these high mixing ratios. I find that the study provided hints as to the cause of the high mixing ratios, but did not provide complete attribution. The analysis would benefit from conducting box model chemistry calculations to fully understand the processes affecting hydroperoxide mixing ratios. In addition, there are a number of items that need further work as detailed below.

Specific Science Comments
1. The abstract should be more quantitative in their claim about enhancements in the AMA versus NH background. Line 22 states that observations show enhanced mixing ratios for H2O2, MHP (CH3OOH), and UHP (unidentified hydroperoxides) in the AMA relative to the NH background. However, Figure 4 shows perhaps a small enhancement (10-20%) of H2O2, which is within the uncertainty (25%) of the measurements and no enhancement of MHP. There is only substantial enhancement (78%) of UHP. More convincing are the histograms in Figure 9 that show median values of H2O2 in the AMA to be 55% higher than those in the NH background, but MHP median values are quite similar between AMA and NH background. Again, the UHP median value is clearly enhanced in the AMA.

Abstract changed to:
Line 22: We observed enhanced mixing ratios of H2O2 (45%), MHP (9%) and UHP (136%) in the AMA relative to the northern hemispheric background. Highest concentrations for H2O2 and MHP of 211 ppbv and 152 ppbv, respectively were found in the tropics outside the AMA, while for UHP, with 208 pptv highest concentrations were found within the AMA. In general, the observed concentrations are higher than steady-state calculations and EMAC simulations. Especially in the AMA, EMAC underestimates the H2O2 (medians: 71 pptv vs. 164 pptv) and ROOH (medians: 25 pptv vs. 278 pptv) mixing ratios.

2. Introduction. Consider adding more information on the flow patterns of the Asian monsoon. A good resource for this information is Lawrence and Lelieveld ACP (2010).

Introduction changed to:
Line 66: So far we know that the updrafts of the summer monsoon deep convection can effectively transport insoluble pollutants from the surface to the upper troposphere and there these polluted air masses can be transported over a long distance (Lawrence and Lelieveld, 2010). Thus the Asian summer monsoon has a strong influence on the upper troposphere (UT)

and the lower stratosphere (Randel et al., 2010; Gettelman et al., 2004) and it is important to study its physical and chemical properties in greater detail.

3. Section 3.1 describes the hydroperoxide measurements. The method measures total peroxides which is the sum of H2O2, CH3OOH, and other organic peroxides. The method uses a catalase to destroy H2O2 allowing the ability to infer H2O2 (i.e. total peroxides minus ROOH gives H2O2, where ROOH represents the sum of organic peroxides). ROOH is assumed to be mainly CH3OOH. To determine CH3OOH, a photostationary-state chemistry approximation is used based on measurements of OH, HO2, CO, CH4, NO, and photolysis rates. It is unclear why it is valid to estimate CH3OOH from photostationary steady-state when the chemical lifetimes of CH3OOH and H2O2 are a few days (as stated on line 381, page 13). It would be better to describe the measurement technique as measuring total peroxides, inferring H2O2, and estimating MHP_PSS with the remaining ROOH being called unidentified hydroperoxides (UHP). Then, when the authors suggest that most of the UHP is CH3OOH, then they can use MHP without further notation.

As mentioned in the experimental section, the ROOH measurement is unspecific and due to the different solubilities of hydroperoxides qualitative. In order to estimate the amount of MHP, which according to previous measurements is expected to be the dominant (if not the only) ROOH component, we calculated the amount of MHP from a photo-stationary state calculation (as well as H2O2). The difference between ROOH and PSS MHP is unexplained or unaccounted for, thus we named it UHP. As discussed in the paper UHP can be due to an unidentified hydroperoxide (e.g. PAA), additional MHP due to advection or a combination of both. Since no specific ROOH measurements were made nor does the 3D-model indicate substantial amount of hydroperoxides other than MHP, we cannot finally decide on the nature (or composition) of the UHP.

4. Lines 295-305. The correlation between UHP and acetone is very strong, but there's no explanation on what the cause and effect may be. I suggest further analysis on this result. Even stating acetone photolysis produces methyl peroxy radical which can react with HO2 to form CH3OOH is good, but more interesting would be box model calculations.

We calculated the production of MHP from acetone and acetaldehyde. For the AMA appr. 40 ppt_v MHP per day can be formed through this reaction.

Section changed to.
L347: Enhanced mixing ratios of hydroperoxides are typically associated with enhanced acetone mixing ratios, especially for PSS-UHP. Our calculation of the production of MHP from the photolysis of acetone and the reaction of acetaldehyde (from EMAC) with OH shows that per day appr. 40 pptv MHP can be formed within the AMA. The lifetime of MHP was calculated to be around 1.5 days. Thus not all of the PSS-UHP in the AMA (median 210 pptv) can be accounted for MHP that was chemically produced from VOCs in the AMA.

5. Section 4.3. I think assuming photostationary steady-state for H2O2 and CH3OOH interferes with the comparisons described in Section 4.3.
a. While, it is useful to point out the large discrepancy between observed H2O2 and H2O2 estimated by photostationary steady-state, it needs an explanation of why there is such a discrepancy (Lines 333-340).

The discrepancy is mainly due to transport phenomena especially deep convection over India.

We added to Section 4.3.1.:
L363: The discrepancy between in situ and PSS-H2O2 shows that the local PSS does not account all main contributions of H2O2 even though all chemical reactions are included. Thus transport phenomena like deep convection seem to play a key role (see 4.3.3).

b. In Section 4.3.2, I do not find it useful to compare the ranges of the observations and EMAC results. For example, EMAC clearly underpredicts CH3OOH mixing ratios most of the time, but the range of EMAC results overlaps with the observations. It may be better to discuss medians or simply describe that most EMAC CH3OOH is < 50 pptv for NH background and AMA air, while most observations range from level of detection to 120 pptv.

Section changed to:
Line 375: EMAC mainly simulates MHP mixing ratios lower than 50 pptv for background and AMA, while PSS-MHP ranges from LOD–140 pptv.

c. The photostationary steady-state assumption interferes with the comparisons of the MHP and UHP observations with EMAC. If H2O2 and CH3OOH are not in photostationary steady-state, then it would make more sense to compare total organic peroxides between observations and EMAC results. The differences between model results and observations need an explanation of why they are different.

In sum we compare total observed peroxides with EMAC-the mixing ratios are just splitted into PSS-MHP from local CH4 oxidation and other organic hydroperoxides. If this is MHP from other chemical sources (e.g. from acetone photolysis or reaction of acetaldehyde and OH), transported MHP or if it is another hydroperoxide like PAA cannot be verified.
Reasons for the differences between the model and observations are given in Lines 432–440:
"Although there is rather good agreement between EMAC simulations and observations for all the species that affect the local photochemical budget of H2O2, EMAC significantly exceeds PSS calculation for H2O2. This is an indication that an additional H2O2 source is accounted for in the global model and that the local photo-stationary-state assumption is not fulfilled. The additional source is attributed to transport associated with deep convection over India, yielding in an upwind source of H2O2 that is significant throughout the western part of the AMA. In the AMA, clouds are absent, so that gas phase photochemical processes may determine the lifetime of H2O2. Based on observed OH levels and photolysis frequencies during OMO the H2O2 lifetime in the upper troposphere is of the order of several days, sufficiently long for the excess H2O2 to reach the western parts of the AMA, producing the observed longitudinal H2O2 gradient observed in both observations and EMAC simulations (Figure 16)."

Sections changed to:
Line 454: Differences between H2O2 observations and EMAC simulations are most likely due to an overestimation of scavenging in the model as also pointed out by Klippel et al., 2011). To investigate this assumption we performed a sensitivity study with EMAC excluding scavenging. The result is shown in Figure 19. The H2O2 mixing ratios significantly increase with longitude by a factor of 3–4 and thus to the level of observed H2O2.

Line 458: There is a rather large uncertainty regarding the scavenging efficiency of MHP in deep convection (Barth et al., 2016). For the Trace A campaign Mari et al. (2000) found observed (modelled) enhancement ratios of post-convective to pre-convective mixing ratios of 11 (9.5) for MHP and 1.9 (1.2) for H2O2. Such efficient transport in the Indian Summer Monsoon would yield a strong source of upper tropospheric MHP explaining the large enhancement of ROOH in the AMA described here. It seems that a large part of the PSS-UHP is actually MHP advected

throughout the AMA after deep convective transport over India. In the EMAC simulations the transport of MHP is less efficient and thus EMAC-MHP is lower than PSS-MHP and PSS-UHP.
d. Shouldn't a conclusion be that assuming photostationary steady-state can be inappropriate?

Yes we would like to stress this in the conclusions. Local photochemistry does not explain the high mixing ratios that we found. Thus transport must play a substantial role especially since other chemical formation of MHP is insufficient. We assume that deep convection is the reason for the higher concentrations in the upper troposphere.

6. Lines 379-385. This discussion, to me, is not well supported and contains a lot of suppositions. This manuscript is relying on one paper (Bozem et al., 2017) to say H2O2 is enhanced in convective outflow regions compared to the background upper troposphere. Yet Bozem et al. (2017) found an unusually high H2O2 mixing ratio in convective outflow (1.25 ppbv) which is not found in other studies. Snow et al. (2007) and Barth et al. (2016) both show that H2O2 is depleted in convective outflow compared to background upper troposphere. We do not know what H2O2 mixing ratios are like in convective outflow near the convection that transports constituents into the AMA, but we can make use of the array of literature from past studies to guide us for what to expect and what further analysis is needed. This leads to my next comment.

We now show the inconsistent results from both sides.

Section changed to:
L403: Previous studies present results that are difficult to reconcile. Snow et al. (2007) and Barth et al. (2016) for example both show that H2O2 is depleted in convective outflow compared to background upper troposphere. In contrast, other studies found that deep convection can be a source of H2O2 in the upper troposphere (e.g. Jaeglé et al., 1997; Prather and Jacob, 1997; Mari et al., 2003; Bozem et al., 2017).

7. There will always be some variability in peroxides scavenging efficiencies and uncertainty in these scavenging efficiencies due to the complex processes associated with convection and chemistry. However, there were also 100s km (multiple days) of transit between the convection in northern India and the measurements over the Arabian Sea. What chemistry occurred during this transit? If it is true that the observations are reflecting chemistry in convective outflow then one would also expect other volatile organic compounds, CO, and CH4 to have been lofted in the convection. I would recommend conducting a number of box model calculations (e.g. Pickering et al., JGR, 1992; Apel et al., ACP, 2012, etc) to learn what chemical transformations are affecting the peroxides. Further, this box model can more definitively provide information on what unidentified hydroperoxides are.

We do not see any chance to get more information on the organic hydroperoxides since PAN and acetaldehyde were not measured during the campaign. Calculations based on EMAC acetaldehyde and observed acetone are added (see above).

8. Lines 405-409. I do not think the typhoon Mireille case is suitable to compare to this paper's results. Typhoon Mireille occurred over the Western Pacific ingesting air from Oceania (Preston et al., JGR, 2019) in the early 1990s and not the South Asia region of the mid 2010s.

We do not want to exactly compare the Typhoon study with our study. We just want to mention that such phenomena are already known from previous studies.

9. I am surprised there is no mention of past literature on peroxides, peroxy radicals and convection and how these current results compare to those previous findings. Some papers to

discuss are Jaeglé et al., GRL, 1997, Prather and Jacob, GRL, 1997, Crawford et al., JGR, 1999).

Some of these studies are now mentioned (see 6.).

Organization, Clarity, Technical Comments
1. Line 140 should include a list of all species measured. It should state OH and HO2 instead of HOx, and include NO.

Section changed to:
L144: For this study CO, CH4, OH, HO2, O3, Acetone, NO, NOy, JH2O2 and JMHP data measured by other instruments have been used for data interpretation, steady-state calculations and interference corrections (see section 3.1). A complete list of all measured compounds can be found in Lelieveld et al., 2018.

2. Lines 192-195. Shouldn't pressure and temperature measurements also be listed? These state parameters must be needed for calculating rate constants and air density.

Section changed to:
L196: Latitude, longitude and altitude data as well as temperature and pressure were collected with the BAHAMAS (BAsic HALO Measurement And Sensor system) instrument. More detailed information about the installation of scientific instruments and mission flights can be found on http://www.halo.dlr.de/science/missions/omo/omo.html.

3. Line 209. It would be good to explain why the CH3O2 to HO2 ratio is needed. It would also be good to define P(HO2) and P(CH3O2).

P(CH3O2) and P(HO2) are defined in eq. 12. As it is analogous to P(H2O2) and P(MHP) we thought this is enough explanation. If not-we can change it.

4. Line 217. Why is a scale height needed? Why not use pressure measurements from the aircraft along with temperature to get air density that can then be translated to N2?

Section changed to:

L220: For the calculations of the rate coefficients the mean temperature of 259.18 K, the mean altitude of 10,992.8 m and the mean pressure of 22,932.9 Pa were used.

5. Line 221. Isn't there a H2O dependence to the self-reaction of HO2? See, for example, JPL (2015). https://jpldataeval.jpl.nasa.gov/

Yes there is a [H_2O] dependence. But in this case it was neglected because of the low RH in the upper troposphere. An example: For 100 ppm H_2O a factor of {1+1.4x10^{-21}*[H2O]*exp(2200/T)} and thus 1.004 needs to be included to the calculation.
(http://iupac.pole-ether.fr/htdocs/datasheets/pdf/HOx14_2HO2_(M).pdf)

Section changed to:
L222: As the relative humidity is very low in the upper troposphere the water dependence in eq. 11 was neglected.

6. Line 229. Can you show or quantify the contribution of CH4+OH and CO+OH to the total CH3O2 and HO2 production, respectively? If the hypothesis is that the higher AMA mixing ratios

are due to convective transport, then HCHO, CH3OOH, and other VOCs will be elevated compared to background mixing ratios and their chemistry may be more important than assumed here.

Section changed to:
Line 234: This is justified by the generally low mixing ratios of these species at high altitudes. Measurements of HCHO with the TRISTAR instrument yielded values below the detection limit of 30 pptv, and although acetaldehyde was not measured, we assume that its mixing ratio is within a factor of two of those of HCHO.

7. Lines 245-248. What grid spacing is used for EMAC? Perhaps a short summary of the configuration could be given in supplemental material. Further, how do the authors analyzed EMAC output to provide comparisons to aircraft observations? Are the model results interpolated in time and space to the aircraft location? Or are values from the nearest grid point and model output time (which, I assume, is every hour)?

The EMAC simulation was made for the flight track of the aircraft. EMAC data were compared to measurements and calculations for the same time and thus location in 2.8°x2.8° grids of the aircraft. Therefore the corresponding values out of the 1 minute means were used. EMAC offers one value every 12 minutes.

Line 253: For this study EMAC simulations were performed for the OMO flight tracks in 2.8°x2.8° grids with a time resolution of 12 minutes. Detailed specifications and results have been published previously (Lelieveld et al., 2018; Tomsche et al., 2019).

Line 276: To compare the simulations from EMAC with measured and PSS calculated data, the corresponding values (out of the 60-second-means) were used at the given times from EMAC.

8. Lines 249-255. What is the procedure when the back-trajectory encounters convection? Does FLEXPART have a means to represent convective transport? Or are the trajectories stop when convection is encountered?

Convective transport can be simulated in FLEXPART with the convection parameterization by Emanuel and Zivkovic-Rothman (1999). To represent moist convection realistically in models, the parametrization includes cloud microphysical processes, the physics of entrainment and mixing, as well as large scale control of ensemble convective activity. It builds on temperature and humidity fields to provide mass flux information (Stohl et al., 2005). The back trajectories in the present paper are calculated with the convective parametrization. Further the Lagrangian particle dispersion model FLEXPART produces so called centroid trajectories, which found on cluster analysis. These trajectories are comparable to traditional trajectories, but include convection via the centroid of all particles per time step.

Section changed to:
L256: Ten-day back-trajectories were calculated along the flight path using FLEXPART to identify the air mass origin (Tomsche et al., 2019). Convective transport can be simulated in FLEXPART with the convection parameterization by Emanuel and Zivkovic-Rothman (1999). To represent moist convection realistically in models, the parametrization includes cloud microphysical processes, the physics of entrainment and mixing, as well as large scale control of ensemble convective activity. It builds on temperature and humidity fields to provide mass flux information (Stohl et al., 2005). The back trajectories in the present paper are calculated with the convective parametrization. Further, the Lagrangian particle dispersion model FLEXPART produces so called centroid trajectories, which found on cluster analysis. These trajectories are

comparable to traditional trajectories, but include convection via the centroid of all particles per time step.

References:

Emanuel, K. A. and Zivkovic-Rothman, M. (1999). Development and Evaluation of a Convection Scheme for Use in Climate Models. Journal of the Atmospheric Sciences, 56(11):17661782.

Stohl, A., Forster, C., Frank, A., Seibert, P., and Wotawa, G.: Technical note: The Lagrangian particle dispersion model FLEXPART version 6.2, Atmos. Chem. Phys., 5, 2461–2474, https://doi.org/10.5194/acp-5-2461-2005, 2005.

9. Line 253-254. Since methane and its use for identifying AMA air via a threshold value is discussed on these lines, it would be useful to combine the first paragraph of section 4.1 with this information. Or move lines 252-255 to section 4.1.

Sentences shifted to 3.5

Line 267: Thus a threshold of CH4≥1879.8 ppbv was used to distinguish between air masses influenced by the monsoon (CH4≥1879.8 ppbv), the SH background (CH4<1820 ppbv) and the NH background (1820 ppbv≤CH4<1879.8 ppbv) (Tomsche et al., 2019).

10. Line 262. It is not clear which species concentrations are binned into 10 pptv segments. Please specify which species.

Section changed to:
L275: For the histograms the concentrations of all species shown were binned into samples with a width of 10 pptv, starting the plots with the lowest bin.

11. Line 265. "Case study: flight 17" is not very descriptive to the general audience. Consider using a heading that mentions the date and location of the flight.

Header changed to:
L278: 4.2 Case study: Flight 17 from Gan to Bahrain (10.08.2015)

12. Line 266. There should also be a short description of the flight, again mentioning date, but perhaps adding weather conditions (cloudy anywhere?) and location of the anticyclone, etc. You might want to add this description to section 2.

Yes there were some clouds but as the focus is on the upper troposphere and the convection took place before and somewhere else it was not mentioned.

Section changed to:
L279: In a case study analyzing flight 17 from 10th of august 2015, the method used to determine the origin of the measured air masses and a quantification and comparison of measured and simulated mixing ratios of H2O2, PSS-MHP and PSS-UHP is presented.

L286: Figure 3 shows the time series for measured H2O2 during the flight at the time steps given from the frequency of EMAC output (orange circles).

13. Line 272. –> Tomsche et al. (2019) and on line 273, remove (Tomsche et al. 2019).

Section changed to:
L285: Tomsche et al. 2019 showed that the measured air in the AMA was affected by deep convection over India resulting in methane mixing ratios above the threshold.

14. Line 274. State what EMAC time step is. I imagine this is the frequency of model output.

Section changed to:
L286: Figure 3 shows the time series for measured H2O2 during the flight at the time steps given from the frequency of EMAC output (orange circles).

15. Line 279-280. Clarify that it is EMAC model data.

Section changed to:
L292: One hour later the EMAC model data decrease to 416 pptv and the in situ data increase to 214 pptv.

16. Line 282. –> last period of the flight at the higher altitude,

Section changed to:
L293: During the following hour until around 8:00 UTC and thus at higher altitude, both mixing ratios increase with the modelled data showing a much stronger increase up to approximately 800 pptv while the in situ data increase only to 230 pptv.

17. Line 293. I think it would be better to say "temporal pattern" rather than "evolution" as there is no following an air parcel in time in the figure.

Section changed to:
L306: The *in situ* H_2O_2 mixing ratios show a similar temporal pattern and mixing ratio levels to those of PSS-UHP over the Arabian Sea and the Arabian Peninsula, with values in the range of 140–243 ppt_v.

18. Line 318. –> is found. Air masses

Section changed to:
L334: For PSS-MHP (Figure 9, middle panel) the frequency distribution in the NH background shows a maximum at 30–40 pptv (green). For AMA influenced air a sharp maximum at 50–70 pptv (red) is found. Air masses from the SH exhibit a rather flat distribution with a maximum at values of 40–50 pptv and a median of 152 pptv (blue).

19. Line 333. –> photostationary steady-state
Section changed to:
L355: A scatter plot of the results from the H2O2 photostationary steady-state calculation based on observed HOx data in the UT (eq. 15) is shown in Figure 12.

20. Line372. It should be degrees E (not O), and please mention the red box in the figure.

Section changed to:

L395: In Figure 16 observations, steady-state calculations and EMAC simulations for upper tropospheric (9–15 km) H2O2 are displayed as a function of longitude from west to east (20–30 °N, 36–60 °E, according to the red box in Figure 15).

21. Line 373. The observations are in orange (not yellow).

Section changed to:
L297: The observations (orange) show roughly a 100% increase of in situ H2O2 from west to east (90 pptv to 175 pptv), similar to simulation with EMAC (black), although absolute mixing ratio levels in EMAC-H2O2 are smaller (61 pptv to 121 pptv).

Figures and Table
1. Consider putting some figures into one with panels.

As the other referee asked for more figures we want to decide this at the end.

2. Figure 2. Please add number of days for back trajectories to caption. It would be helpful to mark each hour (text box of time) along the flight track so one can connect the map to the time series.

Figure changed to:

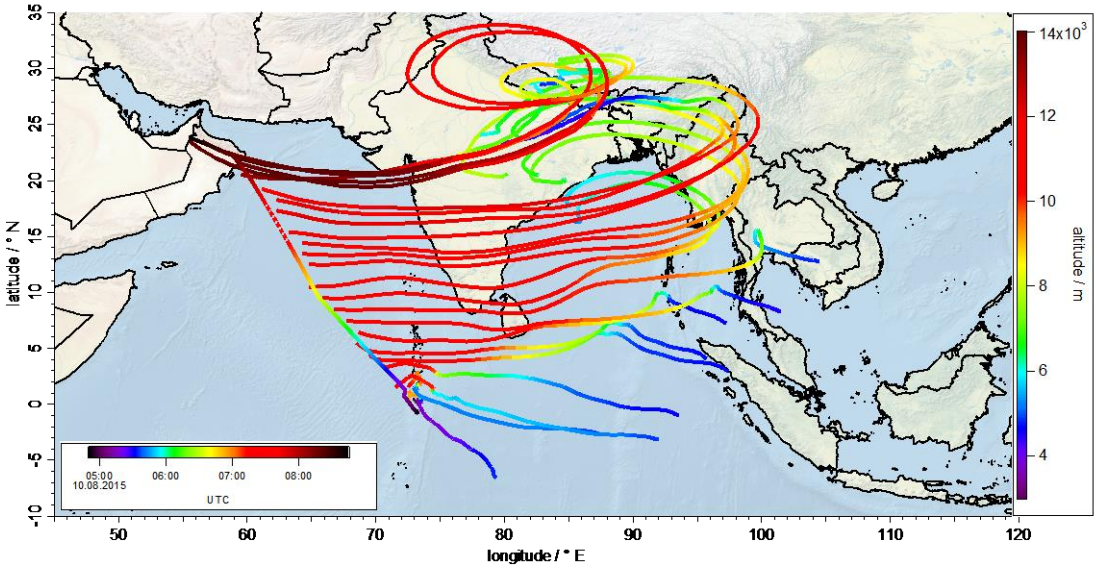

3. Figure 3 and others. It would help to say "EMAC modelled" for clarity. And "dataconstrained calculated" should be "photostationary steady state calculated". At least be consistent from figure to figure and figure to text with nomenclature.

Changed to:
Figure 3: Time series of measured (orange circles), PSS calculated (blue crosses) and modelled (grey triangles) H2O2 mixing ratios for flight 17. The brown line shows the altitude, the colored bar on top indicates the origin of air masses according to the methane mixing ratio classification: for SH blue, NH green and monsoon red.

Figure 4: Time series of hydroperoxide mixing ratios during flight 17. The mixing ratios of in situ H2O2 (orange circles), PSS-MHP (purple triangles) and PSS-UHP (black crosses) are shown.

The brown line shows the altitude, the colored bar on top indicates the origin of air masses according to the methane mixing ratio classification: for SH blue, NH green and monsoon red.

Figure 5: Time series of PSS-UHP (black crosses) and in situ acetone (green circles) mixing ratios during flight 17. The brown line shows the altitude, the colored bar on top indicates the origin of air masses according to the methane mixing ratio classification: for SH blue, NH green and monsoon red.

Figure 6: Scatter plots of measured acetone and in situ H2O2 (left), in situ ROOH (middle) and PSS-UHP (right) during flight 17. The black lines represent the least orthogonal distance fits with regression coefficients of 0.99, 0.98 and 0.99.

Figure 7: Scatter plots of in situ H2O2 (left), in situ ROOH (middle) and PSS-UHP (right) and NO/NOy ratio during flight 17.

Figure 8: All flight positions in the upper troposphere (p<300 hPa) during OMO as a function of (a) in situ H2O2 on top, (b) PSS-MHP in the middle and (c) PSS-UHP at the bottom.

Figure 9: Histograms of in situ H2O2 (top), PSS-MHP (middle) and PSS-UHP (bottom) mixing ratios during the OMO campaign for NH background (green), SH (blue) and monsoon (red) air masses.

Figure 10: Scatter plots of in situ acetone and in situ H2O2 (left), in situ ROOH (middle) and PSS-UHP (right) in the UT (purple squares) and especially in the AMA (red circles). The black lines represent the least orthogonal distance fit with linear regression coefficients of 0.96 (H2O2), 0.97 (ROOH) and 0.96 (UHP).

Figure 11: Scatter plots of NO/NOy and in situ H2O2 (left), in situ ROOH (middle) and PSS-UHP (right) in the UT (blue triangles) and especially in the AMA (red circles).

Figure 12: Scatter plot of in situ and PSS calculated H2O2 mixing ratios (red) with the 1:1 (black), 1:2 and 2:1 (both green) lines.

Figure 13: Histograms of in situ (top) and PSS (bottom) H2O2 mixing ratios (bars) and the associated medians (lines).

Figure 14: Histograms of in situ and EMAC H2O2 (top), PSS and EMAC-MHP (middle) and PSS and EMAC-UHP (bottom) mixing ratios during the OMO campaign for NH background (green), SH (blue) and AMA (red) air masses.

Figure 16: Longitudinal trends of in situ H2O2 mixing ratios (orange circles), EMAC-H2O2 (black triangles) and PSS H2O2 (purple crosses). The data are shown in the light colors while the darker ones represent the medians.

Figure 17: Longitudinal trends of in situ ROOH mixing ratios (green asterisks), EMAC-ROOH (blue plus signs) and PSS mixing ratios for MHP (pink triangles) and UHP (black crosses) as well as EMAC-MHP (yellow squares). The data are shown in the light colors while the darker ones represent the medians.

Figure 18: Scatter plot of in situ and EMAC HO2 data (left) and the OH data (right) (both red) with the 1:1 (black), 1:2 and 2:1 (both green) lines. The blue line shows the calculated least orthogonal distance fit.

Figure 19: Longitudinal trends of in situ H2O2 mixing ratios (orange circles), EMAC (black triangles) and the sensitivity study without scavenging in EMAC (blue circles). The data are shown in the light colors while the darker ones represent the medians.

4. Figure 4. Purple triangles look red in my version.

Might be due to the printer used.

5. Figures 5, 6 and 7 could be combined. The lilac colored squares should be darker.

As figures 6 and 7 are now made of 3 scatter plots we do not combine these figures.

6. Figure 8. Please note in the figure caption that you are showing data only at <300 hPa.

Caption changed to:
Figure 8: All flight positions in the upper troposphere (p<300 hPa) during OMO as a function of (a) in situ H2O2 on top, (b) PSS-MHP in the middle and (c) PSS-UHP at the bottom.

7. Figures 10, 11, and 12 could be combined. The lilac colored squares should be darker.

As figures 10 and 11 are now made of 3 scatter plots we do not combine these figures.

8. Figure 12 figure caption should say "photostationary steady state calculated".

Caption changed to:
Figure 12: Scatter plot of in situ and PSS calculated H2O2 mixing ratios (red) with the 1:1 (black), 1:2 and 2:1 (both green) lines.

9. Figure 14 axes labels and legends need to be larger. Please explain what vertical lines are in the caption.

Vertical lines are explained in the legend-these are medians. Font size now increased.

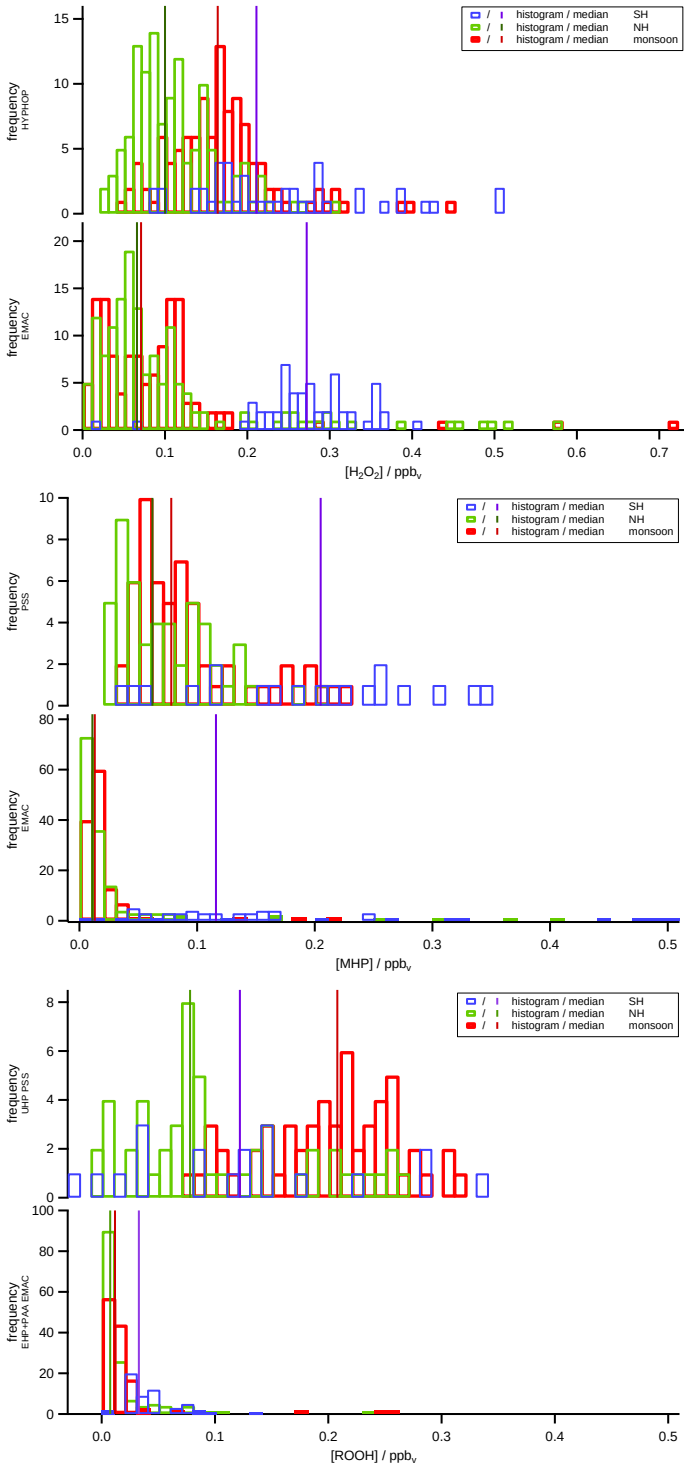

Figure 1: Histograms of observed and modelled H_2O_2 (top), MHP (middle) and UHP (bottom) mixing ratios during the OMO campaign for NH background (green), SH (blue) and AMA (red) air masses.

10. Figure 15. Please explain what the red box is in the caption.

Caption changed to:

Figure 15: Location of measurements used for the longitudinal gradient study (red box) out of all flight tracks (black).

11. Figure 16. The photostationary steady state calculated markers are purple not blue.

Caption changed to:
Figure 16: Longitudinal trends of in situ H2O2 mixing ratios (orange circles), EMAC-H2O2 (black triangles) and PSS H2O2 (purple crosses). The data are shown in the light colors while the darker ones represent the medians.

12. Figure 17. The MHP mixing ratios look more like pink than purple.

Caption changed to:
Figure 17: Longitudinal trends of in situ ROOH mixing ratios (green asterisks), EMAC-ROOH (blue plus signs) and PSS mixing ratios for MHP (pink triangles) and UHP (black crosses) as well as EMAC-MHP (yellow squares). The data are shown in the light colors while the darker ones represent the medians.

13. Table 1. Are these values from all flights? Please say so in the caption. "calc." is not a good heading. I suggest PSS estimate.

Table changed to:

Table 2: Comparison of H_2O_2, MHP and UHP mixing ratios in the upper troposphere from EMAC, measurements and PSS calculations.

region	median	$[H_2O_2]/ppt_v$		$[MHP]/ppt_v$		$[UHP]/ppt_v$	
		EMAC	HYPHOP	EMAC	PSS	EMAC	PSS
NH background	median	66	100	11	64	8	78
	range	6–576	20–301	2–408	21–202	1–238	LOD–261
	avg±sdev	102±110	110±53	28±58	75±42	18±31	103±77
monsoon	median	71	164	13	70	12	208
	range	8–714	46–446	2–216	37–220	1–259	80–311
	avg±sdev	84±92	167±69	18±28	92±49	18±34	199±59
SH background	median	272	211	116	152	33	122
	range	15–409	85–510	2–502	40–346	1–132	LOD–334
	avg±sdev	272±68	238±105	155±125	191±95	42±24	125±102

Impact of the South Asian monsoon outflow on atmospheric hydroperoxides in the upper troposphere

Bettina Hottmann[1], Sascha Hafermann[1], Laura Tomsche[1*†], Daniel Marno[1], Monica Martinez[1], Hartwig Harder[1], Andrea Pozzer[1], Marco Neumaier[2], Andreas Zahn[2], Birger Bohn[3], Greta Stratmann[4], Helmut Ziereis[4], Jos Lelieveld[1] and Horst Fischer[1]

[1]Atmospheric Chemistry Department, Max Planck Institute for Chemistry, Mainz, 55128, Germany
[2]Karlsruhe Institute of Technology, Karlsruhe, 76021, Germany
[3]Forschungszentrum Jülich GmbH, Jülich, 52425, Germany
[4]German Aerospace Center, Institute of Atmospheric Physics, Oberpfaffenhofen, 82234, Germany
[*]now at NASA Langley Research Center, Hampton, VA 23681, USA
[†]now at Universities Space Research Association, Columbia, MD 21046, USA
Correspondence to: Bettina Hottmann (Bettina.Hottmann@mpic.de) and Horst Fischer (Horst.Fischer@mpic.de)

Abstract. During the OMO (Oxidation Mechanism Observation) mission, trace gas measurements were performed onboard the HALO (High Altitude LOng range) research aircraft in summer 2015 in order to investigate the outflow of the south Asian summer monsoon and its influence on the composition of the Asian Monsoon Anticyclone (AMA) in the upper troposphere over the eastern Mediterranean and the Arabian Peninsula. This study focuses on *in situ* observations of hydrogen peroxide (H_2O_2) and organic hydroperoxides (ROOH), as well as their precursors and loss processes. Observations are compared to steady state calculations of H_2O_2, methyl hydroperoxide (MHP) and inferred unidentified hydroperoxide (UHP) mixing ratios. Measurements are also contrasted to simulations with the general circulation ECHAM/MESSy for Atmospheric Chemistry (EMAC) model. We observed enhanced mixing ratios of H_2O_2 (45%), MHP (9%) and UHP (136%) in the AMA relative to the northern hemispheric background. Highest concentrations for H_2O_2 and MHP of 211 ppb_v and 152 ppb_v, respectively were found in the tropics outside the AMA, while for UHP, with 208 ppt_v highest concentrations were found within the AMA. In general, the observed concentrations are higher than steady-state calculations and EMAC simulations. Especially in the AMA, EMAC underestimates the H_2O_2 (medians: 71 ppt_v vs. 164 ppt_v) and ROOH (medians: 25 ppt_v vs. 278 ppt_v) mixing ratios. Longitudinal gradients indicate a pool of hydroperoxides towards the center of the AMA, most likely associated with upwind convection over India. This indicates main contributions of atmospheric transport to the local budgets of hydroperoxides along the flight track, explaining strong deviations to steady-state calculations which only account for local photochemistry. Deviations to EMAC simulations are most likely due to uncertainties in the scavenging efficiencies for individual hydroperoxides in deep convective transport to the upper troposphere, corroborated by a sensitivity study. It seems that the observed excess UHP is excess MHP transported to the west from an upper tropospheric source related to convection in the summer monsoon over South-East Asia.

1 Introduction

The earth has an oxidizing atmosphere where OH functions as the main oxidizing agent (Levy, 1971). OH is formed by the photolysis of ozone (λ<320 nm) and subsequent reaction of the produced singlet D

oxygen atom (O^1D) with water vapor. The main sinks of OH are also the main sources of peroxy radicals (HO_2 and RO_2) in the reactions with CO, CH_4 and volatile organic compounds (VOCs) and the reaction with nitrogen dioxide (NO_2) to form nitric acid (HNO_3). At low NO_x ($NO+NO_2$) concentrations, HO_2 reacts with itself to form H_2O_2 or with RO_2 to form organic hydroperoxides (ROOH). Since HO_2 and RO_2, especially CH_3O_2, react faster with NO than with HO_2, peroxides are mainly produced in areas with low NO and high OH mixing ratios (Lee et al., 2000). H_2O_2 is a strong oxidant in the aqueous phase, oxidizing for example SO_2 to H_2SO_4, and hence H_2O_2 partially contributes to acid rain formation (e.g. Hoffmann and Edwards, 1975; Penkett et al., 1979; Robbin Martin and Damschen, 1981; Calvert et al., 1985). The major photochemical sinks of hydroperoxides are photolysis, which recycles OH, and the reaction with OH forms HO_2. Physical loss of hydroperoxides due to dry and wet deposition establishes an ultimate loss mechanism of HO_x radicals. Thus H_2O_2 and ROOH play a pivotal role to the HO_x-budget and modulate the oxidation capacity of the atmosphere (Lelieveld and Crutzen, 1990; Crutzen et al., 1999).

The global distribution of hydroperoxides is affected by transport, physical removal by dry deposition and rainout as well as net photochemical production processes. With increasing altitude, and thus decreasing water vapor concentration, the primary production of HO_x decreases (Heikes et al., 1996) and leads to an increasing contribution of the photolysis of H_2O_2 and ROOH to the HO_x budget (Jaeglé et al., 1997; Jaeglé et al., 2000; Faloona et al., 2000; Faloona et al., 2004). In more polluted areas, especially in the boundary layer, the H_2O_2 chemistry is more complex and leads to higher variabilities (Nunnermacker et al., 2008). Close to the surface dry deposition of H_2O_2 forms a strong sink resulting in decreasing concentrations with decreasing altitude. This often leads to a local maximum of H_2O_2 mixing ratios above the boundary layer at 2–5 km of altitude (Daum et al., 1990; Heikes, 1992; Weinstein-Lloyd et al., 1998; Snow, 2003; Snow et al., 2007; Klippel et al., 2011). A similar but weaker maximum at 2–5 km was found for methyl hydroperoxide (MHP) (Weinstein-Lloyd et al., 1998; Snow, 2003; Snow et al., 2007). Due to its lower deposition velocity associated with less efficient uptake by solid and aqueous surfaces, MHP is not as sensitive to deposition processes as H_2O_2 (Lind and Kok, 1986, 1994), yielding rather constant mixing ratios with altitude within the boundary layer. Further, the mixing ratios of both species generally decrease with increasing latitude in the free troposphere due to lower water vapor concentrations (Jacob and Klockow, 1992; Perros, 1993; Slemr and Tremmel, 1994; Snow, 2003; Snow et al., 2007; Klippel et al., 2011).

In spite of several *in situ* measurement campaigns of trace gases in the outflow of the Asian summer monsoon in the recent years, e.g. from the IAGOS-CARIBIC project (Ojha et al., 2016; Rauthe-Schöch et al., 2016), the IAGOS-MOZAIC project (Barret et al., 2016), the MINOS aircraft campaign (Lelieveld et al., 2002) and the PEM-WEST A mission (Heikes et al., 1996) our understanding of the physical and chemical processes within the Asian Monsoon Anticyclone (AMA) is limited. So far we know that the updrafts of the summer monsoon deep convection can effectively transport insoluble pollutants from the surface to the upper troposphere and there these polluted air masses can be transported over a long distance (Lawrence and Lelieveld, 2010). Thus the Asian summer monsoon has a strong influence on the upper troposphere (UT) and the lower stratosphere (Randel et al., 2010; Gettelman et al., 2004) and it is important to study its physical and chemical properties in greater detail.

The focus of the OMO (Oxidation Mechanism Observation) campaign was to investigate photochemical processes in the AMA in the UT. During the mission, HALO probed a large variety of air masses, ranging

from clean northern hemispheric (NH) background air above the western Mediterranean, southern hemispheric (SH) background air over the northern Indian Ocean and air masses affected by the South Asian summer monsoon in the AMA over the Arabian Peninsula. The main goals of the campaign were to analyze the influence of the AMA on the oxidizing power of the atmosphere and to determine the rates at which natural and human-made compounds are converted by oxidation processes in the atmosphere (Lelieveld et al., 2018).

The present study addresses the budgets of H_2O_2 and organic hydroperoxides. Since the measurements of organic hydroperoxides are unspecific, we estimate the contribution from methyl hydroperoxide (MHP) based on steady-state calculations. In former studies MHP was identified as the most abundant organic hydroperoxide in the free troposphere (Heikes et al., 1996; Jackson and Hewitt, 1996). Our goal was to investigate to what extent this is also the case for the outflow of the South Asian summer monsoon into the UT. In addition the *in situ* data were compared to results from the EMAC model (see 3.5) along the flight track for H_2O_2 and individual ROOH mixing ratios. Observed H_2O_2 mixing ratios were also evaluated with steady-state calculations based on measured HO_x and photolysis frequency measurements onboard of HALO.

2 The OMO project

The OMO campaign took place from 21st of July to 27th of August 2015. During the campaign 17 flights with the HALO (High Altitude and LOng range) research aircraft were performed. The airports of Oberpfaffenhofen (Germany), Paphos (Cyprus), Gan (Maldives) and Bahrain served as bases for take-offs and landings. The flights were mainly performed over the Arabian Peninsula, the Eastern Mediterranean and the Northern Indian Ocean (11.3–80.2°E and 0.2°S–48.1°N). In Figure 2 the tracks of all OMO flights are shown. The aircraft reached altitudes up to 15 km which corresponds to 130 hPa to study the chemistry of the UT.

3 Methods

3.1 Hydroperoxide measurements

The hydroperoxide data during OMO were obtained using a modified commercial instrument (AEROLASER, model AL2021, Garmisch-Partenkirchen, Germany) called HYPHOP (HYdrogen Peroxide and Higher Organic Peroxides monitor). The HYPHOP-instrument was installed in a 19'' rack together with the IR-laser absorption instrument TRISTAR (Tracer *In Situ* Tdlas for Atmospheric Research) mounted in the back of HALO. Air was sampled from the top of the aircraft fuselage through a forward-facing trace gas inlet (TGI) designed as a bypass, consisting of a ½'' PFA (perfluoroalkoxy alkanes) tube inside the aircraft with an exit through a second TGI. From this bypass air was sampled at a flow rate of 2 slpm (standard liter per minute) through a ¼'' PFA tube and directed to HYPHOP. To obtain constant pressure at the HYPHOP inlet a constant pressure inlet (CPI) consisting of a dual stage membrane pump (Vacuubrand MD1C VARIO SP, Wertheim, Germany) was used (Klippel et al., 2011).

HYPHOP relies on a dual enzyme detection method after transfer of gaseous hydroperoxides into a buffered solution (potassium hydrogen phthalate/NaOH, pH 6) in a glass stripping coil (Lazrus et al.,

1985; Lazrus et al., 1986). This stripper also contains EDTA (ethylenediaminetetraacetic acid) to prevent the reaction of transition metal ions with the hydroperoxides. Additionally, formaldehyde (HCHO) is added to prevent the oxidation of dissolved SO_2 (in alkaline solutions HSO_3^-) by the hydroperoxides. Instead, HCHO and HSO_3^- form hydroxymethyl sulfonate ($HOCH_2SO_3^-$). After the stripping coil the hydroperoxide containing solution is divided into two channels. Catalase is added to one channel in order to selectively destroy H_2O_2. This first channel thus measures only ROOH, while the second channel (without catalase) measures the sum of ROOH and H_2O_2. Since hydroperoxides cannot be detected by fluorescence directly, a second enzyme (horseradish peroxidase) and *p*-hydroxyphenylacetic acid (POPHA) are added to both channels. In a quantitative and selective reaction the enzyme catalyzes the oxidation of POPHA by hydroperoxides forming the fluorescent dye 6,6'-dihydroxy-3,3'-biphenyldiacetid acid. After excitation at 326 nm with a Cd lamp, the fluorescence at 400–420 nm is detected. To enlarge the fluorescence intensity sodium hydroxide is added.

In order to perform zero measurements, the sampled air is directed through a cylinder filled with hopcalite (MnO_2 and CuO) to eliminate H_2O_2, ROOH and Ozone. Since the efficiency of Hopkalit decreases with increased humidity, the air is dried beforehand with the help of orange gel (SiO_2 beads plus indicator).

To convert the detected signal into a concentration a 4-point calibration was performed before and after every flight. In the first two steps a liquid standard of H_2O_2 (1 µmol/L, freshly diluted from stock solution) followed by zero air is measured in both channels without catalase. Afterwards this is repeated with catalase in the ROOH channel for the last two steps. The sensitivity for both channels and the catalase efficiency are determined via this procedure. The concentration of the liquid standard is based on titration of the stock solution (10 mmol/L) with potassium permanganate.

To determine the stripping efficiency for H_2O_2, a gas phase standard based from a permeation source (Teflon tube filled with 30% H_2O_2 in a temperature-controlled glass flask) is used at a constant flow rate of approximately 40 sccm diluted with synthetic air and measured with the instrument. The permeation rate of the source is quantified by collecting the output of the source into cooled water. The addition of hydrochloric titanium tetrachloride yields the formation of the yellow η^2-peroxo complex $[Ti(\eta^2\text{-}O_2)Cl_4]^{2-}$ (Pilz and Johann, 1974) whose concentration is determined via a UV photometer. The stripping efficiency of MHP was assumed to be 60% and that of H_2O_2 100% (AEROLASER, 2006; Lee et al., 2000).

The inlet efficiency was determined with the help of the permeation source which was measured with and without the CPI. In laboratory studies the inlet efficiency was determined to be 87% ± 3% decreasing during the campaign to 62.7% ± 0.8%, which is mainly due to the higher humidity.

The limits of detection (LOD) and precisions for H_2O_2 and MHP (assuming total ROOH to be mainly MHP), respectively, have been calculated for each flight from the reproducibility (1σ standard deviation) of in-flight zero (650 values) and liquid calibration (100 values) measurements, taking into account the sensitivity, stripping and catalase efficiency. Values for the LOD are in the range of 8–53 ppt_v for H_2O_2 (median 23 ppt_v) and 9–52 ppt_v for MHP (median 23 ppt_v) respectively. Precision values were determined from the reproducibility of standard measurements and are in the range of 0.2%@5.2 ppb_v and 1.3%@5.9 ppb_v for H_2O_2 and 0.3%@5.0 ppb_v and 2.1%@6.0 ppb_v for MHP. The time resolution (signal

increase from 10% to 90%) of the instrument is 120 s. An ozone interference of 53 ppt_v H_2O_2 per 100 ppb_v O_3, which was determined by H_2O_2 measurements in the stratosphere during the OMO-EU test campaign, was taken into account and corrected.

The total uncertainty calculated from statistical errors and uncertainties of liquid standard, inlet and stripping efficiency and ozone interference is 25% for H_2O_2 and 40% for MHP.

3.2 Other *in situ* measurements

For this study CO, CH_4, OH, HO_2, O_3, Acetone, NO, NO_y, J_{H2O2} and J_{MHP} data measured by other instruments have been used for data interpretation, steady-state calculations and interference corrections (see section 3.1). A complete list of all measured compounds can be found in Lelieveld et al., 2018. CO and CH_4 have been measured by the IR-quantum cascade laser absorption spectrometer TRISTAR (Schiller et al., 2008; Tadic et al., 2017). The measurements comprised an ambient air mode and in-flight calibrations. The latter were realized with secondary standards from pressurized bottles (6 L bottle, Auer GmbH, Germany), which were calibrated against certified reference gases (Tomsche et al., 2019). With the help of the in-flight calibrations the *in situ* data are drift-corrected by interpolation between two calibrations (Tadic et al., 2017). The observed CO and CH_4 mixing ratios have a total uncertainty of 5.1% and 0.275%, respectively. The relatively high CO uncertainty reflects problems with the stability of the CO quantum cascade laser during the second half of OMO.

Laser induced fluorescence was the method utilized for HO_x measurements (instrument name: HORUS, Faloona et al., 2004; Martinez et al., 2010). The accuracies of the measurements are 17.1% for OH and 17.6% for HO_2. The limit of detection of the instrument does vary depending on altitude as this system has a sensitivity that depends on pressure. As altitude increases the LOD decreases from 0.1 ppt_v to 0.02 ppt_v for OH and 0.361 ppt_v to 0.175 ppt_v for HO_2.

FAIRO (Fast AIRborne Ozone instrument) is a light-weight (14.5 kg) and accurate 2-sensor device for measuring O_3. It combines two techniques, i.e. (a) a UV photometer that measures the light absorption by O_3 at a wavelength of λ = 250–260 nm emitted by a UV-LED and (b) a chemiluminescence detector that monitors the chemiluminescence generated by O_3 on the surface of an organic dye adsorbed on dry silica gel. These techniques are simultaneously applied in order to combine the high measurement accuracy of the UV photometry with the high measurement frequency of the chemiluminescence detection. The UV photometer has a 1-σ precision of 0.08 ppb_v at a measurement frequency of 0.25 Hz (and a pressure of 1 bar) and an accuracy of 1.5% (determined by the uncertainty of the O_3 cross section). The chemiluminescence detector has a precision of 0.05 ppb_v at a measurement frequency of 12.5 Hz (Zahn et al., 2012). In post-processing the chemiluminescence detector data is calibrated using the UV photometer data.

Nitrogen oxide (NO) and total reactive nitrogen (NO_y) were measured using the AENEAS-atmospheric nitrogen oxides measuring system. The measurements were performed by a dual channel NO-chemiluminescence detector (CLD-SR 790, Eco Physics, Switzerland) in combination with a converter technique for the detection of total reactive nitrogen as NO. NO_y comprises among others NO, NO_2, HNO_3, NO_3, N_2O_5, HNO_2, HO_2NO_2, PAN and organic nitrates. The individual NO_y species were detected after conversion to NO using a gold tube maintained at about 300 °C with H_2 as a reducing agent (Ziereis

et al., 2000). Ambient air was sampled using a standard HALO trace gas inlet equipped with a heated (~ 40 °C) PFA inlet line. The time resolution of the measurements was about 1 s. The overall uncertainty of the NO and NO_y measurements depends on its ambient concentrations and is about 8% (6.5%) for volume mixing ratios of 0.5 nmol/mol (1 nmol/mol), respectively (Stratmann et al., 2016).

VOCs (e.g. acetone) were measured with a homebuilt light-weight (~55 kg without rack) proton-transfer-reaction mass spectrometer which uses a commercial quadrupole mass analyzer (Pfeiffer, QMA 410, Germany). A modular V25 micro computer system (MPI-C, Mainz, Germany) is applied for instrument control and data acquisition. A custom-built inlet system comprises a platinum/quartz wool scrubber (Shimadzu, High Sensitivity Catalyst) held at 300 °C and components for flow and pressure control. The instrument was calibrated between flights with a dynamically diluted gas standard containing approximately 500 ppb_v of VOCs (Apel-Riemer Environmental Inc., USA). The accuracy for acetone is typically ±10% and the detection limit is ~60 ppt_v.

Photolysis frequencies were calculated from spectral actinic flux density spectra (280–650 nm) obtained from CCD spectroradiometer measurements on the top and bottom fuselage of the aircraft covering the upper and the lower hemisphere, respectively (Bohn and Lohse, 2017). Recent recommendations of absorption cross sections and quantum yields were used in the calculations, as well as their temperature and pressure dependencies (if available) by taking into account measured static air temperatures and pressures. Radiometric uncertainties range around 5–6% under typical flight conditions. Additional uncertainties related to the molecular parameters are process specific. For H_2O_2 in particular, recommended absorption cross sections and their temperature dependencies were applied and unity quantum yields were assumed (Burkholder et al., 2015). However, the recommended H_2O_2 absorption cross sections are confined to a wavelength range below 350 nm which is insufficient to capture atmospheric photolysis completely. Because measured cross sections decay exponentially over two orders of magnitude in the range 280–350 nm, this dependence was further extrapolated up to 370 nm where values drop well below 10^{-22} cm^2. Dependent on conditions this extrapolation increases atmospheric H_2O_2 photolysis frequencies by 10–20%. For MHP the temperature dependence of the absorption cross sections is unknown. Therefore the recommended room temperature data were used under all conditions as well as unity quantum yields (Burkholder et al., 2015). Combined total uncertainties of 15% and 25% are estimated for H_2O_2 and MHP photolysis frequencies, respectively.

Latitude, longitude and altitude data as well as temperature and pressure were collected with the BAHAMAS (BAsic HALO Measurement And Sensor system) instrument. More detailed information about the installation of scientific instruments and mission flights can be found on http://www.halo.dlr.de/science/missions/omo/omo.html.

3.3 Photo-stationary state calculations

Since only the sum of organic hydroperoxides was measured we estimated the contribution of MHP using a photo-stationary-state (PSS) approximation relying on *in situ* measurements of HO_2, OH, CO, CH_4, NO, J_{MHP} and J_{H2O2} (see 3.2) and rate coefficient data from Atkinson et al., 2004 and Atkinson et al., 2006).

In the free troposphere the production rate P of H_2O_2 and MHP is due to the self-reaction of HO_2 and reaction of CH_3O_2 with HO_2, respectively, and can be calculated from Eq. 1 and 2.

$$P(H_2O_2) = k_{HO_2+HO_2} \cdot [HO_2]^2 , \quad (1)$$

$$P(MHP) = k_{CH_3O_2+HO_2} \cdot [CH_3O_2] \cdot [HO_2] , \quad (2)$$

Photochemical loss rates L of H_2O_2 and MHP are due to photolysis and reaction with OH according to Eq. 3 and 4.

$$L(H_2O_2) = \left(k_{H_2O_2+OH} \cdot [OH] + J_{H_2O_2}\right) \cdot [H_2O_2] , \quad (3)$$

$$L(MHP) = \left(k_{MHP+OH} \cdot [OH] + J_{MHP}\right) \cdot [MHP] , \quad (4)$$

For steady-state conditions the production and loss reactions are at equilibrium and the MHP to H_2O_2 ratio can be calculated from Eq. 5.

$$\frac{[MHP]}{[H_2O_2]} = \frac{k_{CH_3O_2+HO_2} \cdot [CH_3O_2] \cdot [HO_2]}{k_{HO_2+HO_2} \cdot [HO_2]^2} \cdot \frac{k_{H_2O_2+OH} \cdot [OH] + J_{H_2O_2}}{k_{MHP+OH} \cdot [OH] + J_{MHP}} , \quad (5)$$

Similarly the CH_3O_2 to HO_2 ratio can be deduced from Eq. 6.

$$\frac{[CH_3O_2]}{[HO_2]} = \frac{L(HO_2) \cdot P(CH_3O_2)}{P(HO_2) \cdot L(CH_3O_2)} , \quad (6)$$

Dominant loss processes for HO_2 and CH_3O_2 are reactions with NO and the production of H_2O_2 and MHP, respectively, neglecting the production of peroxy nitrates due to low NO_2 concentrations in the UT (Eq. 7 and 8).

$$L(HO_2) = k_{CH_3O_2+HO_2} \cdot [CH_3O_2] \cdot [HO_2] + k_{HO_2+NO} \cdot [HO_2] \cdot [NO] + k_{HO_2+HO_2} \cdot [HO_2]^2 , \quad (7)$$

$$L(CH_3O_2) = k_{CH_3O_2+HO_2} \cdot [CH_3O_2] \cdot [HO_2] + k_{CH_3O_2+NO} \cdot [CH_3O_2] \cdot [NO] , \quad (8)$$

The first terms on the right side of both equations are identical. The second terms are dominated by the rate coefficients of the reactions with NO and the NO concentration. For the calculations of the rate coefficients the mean temperature of 259.18 K, the mean altitude of 10,992.8 m and the mean pressure of 22,932.9 Pa were used. The resulting values are shown in Eq. 9–11. As the relative humidity is very low in the upper troposphere the water dependence in eq. 11 was neglected.

$$k_{HO_2+NO} = 3.45 \cdot 10^{-12} \cdot \exp^{\frac{270}{T}} = 9.78 \cdot 10^{-12} \frac{cm^3}{molecule \cdot s} , \quad (9)$$

$$k_{CH_3O_2+NO} = 2.3 \cdot 10^{-12} \cdot \exp^{\frac{360}{T}} = 9.22 \cdot 10^{-12} \frac{cm^3}{molecule \cdot s} , \quad (10)$$

$$k_{HO_2+HO_2} = 2.2 \cdot 10^{-13} \cdot \exp^{\frac{600}{T}} + 1.9 \cdot 10^{-33} \cdot [N_2] \cdot \exp^{\frac{980}{T}} = 2.64 \cdot 10^{-12} \frac{cm^3}{molecule \cdot s} , \quad (11)$$

This indicates that the reaction of HO_2 with NO is more than a factor of 3 faster than the self-reaction. The measured NO concentration is an order of magnitude larger than measured HO_2, so that reaction with NO is the dominant process for both HO_2 and CH_3O_2 resulting in similar loss rates for both radicals in the UT. Thus, the ratio of CH_3O_2 to HO_2 is dominated by their production rates (Eq. 12).

$$\frac{[CH_3O_2]}{[HO_2]} = \frac{P(CH_3O_2)}{P(HO_2)} = \frac{k_{CH_4+OH} \cdot [CH_4] \cdot [OH]}{k_{CO+OH} \cdot [CO] \cdot [OH]} , \quad (12)$$

The combination of Eq. 5 and 12 yields in Eq. 13 which was used to calculate the MHP concentrations.

$$[\mathrm{MHP}] = \frac{k_{CH_3O_2+HO_2}}{k_{HO_2+HO_2}} \cdot \frac{k_{H_2O_2+OH}\cdot[OH]+J_{H_2O_2}}{k_{MHP+OH}\cdot[OH]+J_{MHP}} \cdot \frac{k_{CH_4+OH}\cdot[CH_4]}{k_{CO+OH}\cdot[CO]} \cdot [H_2O_2], \quad (13)$$

Please note that other sources of HO_2 and CH_3O_2, in particular the photolysis of formaldehyde (HCHO) and acetaldehyde, respectively have been neglected. This is justified by the generally low mixing ratios of these species at high altitudes. Measurements of HCHO with the TRISTAR instrument yielded values below the detection limit of 30 pptv, and although acetaldehyde was not measured, we assume that its mixing ratio is within a factor of two of those for HCHO.

The total uncertainty of MHP from the calculation according to equation 13 can be deduced from error propagation taking into account uncertainties in rate constants, OH (17.1%), J_{H2O2} (15%), J_{MHP} (25%), CH_4 (0.275%), CO (5.1%) and H_2O_2 (25%) to be of the order of 45% (1σ).

To estimate the composition of the organic hydroperoxides the calculated concentration of MHP was subtracted from the measured sum of all organic hydroperoxides. This leads to a concentration of unidentified organic hydroperoxides (UHP) (Eq. 14).

$$[\mathrm{UHP}] = [\mathrm{ROOH}] - [\mathrm{MHP}], \quad (14)$$

3.4 H_2O_2 calculation

In order to classify the measured H_2O_2, HO_2 and OH data we calculated H_2O_2 from measured HO_x and J_{H2O2}. For the calculation Eq. 15 was used which is based on Eq. 1 and Eq. 3.

$$[H_2O_2]_{PSS} = \frac{[HO_2]^2\cdot k_{HO_2}}{[OH]\cdot k_{OH}+J_{H_2O_2}}, \quad (15)$$

A total uncertainty of 45% (1σ) due to uncertainties in reaction rate constants, OH (17.1%), HO_2 (17.6%) and J_{H2O2} (15%) was calculated.

3.5 Other research tools

The EMAC (ECHAM/MESSy Atmospheric Chemistry) model comprises the 5th generation of the European Center HAMburg (ECHAM5; Roeckner et al., 2006; version 5.3.01) general circulation model and the Modular Earth Submodel System (MESSy; Jöckel et al., 2016; version 2.52, http://www.messy-interface.org/). For this study EMAC simulations were performed for the OMO flight tracks in 2.8°x2.8° grids with a time resolution of 12 minutes. Detailed specifications and results have been published previously (Lelieveld et al., 2018; Tomsche et al., 2019).

Ten days back-trajectories were calculated along the flight path using FLEXPART to identify the air mass origin (Tomsche et al., 2019). Convective transport can be simulated in FLEXPART with the convection parameterization by Emanuel K. A. and Zivkovic-Rothman M., 1999. To represent moist convection realistically in models, the parametrization includes cloud microphysical processes, the physics of entrainment and mixing, as well as large scale control of ensemble convective activity. It builds on temperature and humidity fields to provide mass flux information (Stohl et al., 2005). The back

trajectories in the present paper are calculated with the convective parametrization. Further the Lagrangian particle dispersion model FLEXPART produces so called centroid trajectories, which found on cluster analysis. These trajectories are comparable to traditional trajectories, but include convection via the centroid of all particles per time step. As indicated by Tomsche et al. prominent source regions of AMA air masses are identified to be the Indo Gangetic Plain, Northeast India, Bangladesh and the Bay of Bengal. Additionally, Tomsche et al. used observations of methane to differentiate between air masses influenced by the south Asian summer monsoon and background air. A comparison of vertical profiles indicated that the air inside the AMA showed significantly higher CH_4 concentrations than outside. Thus a threshold of $CH_4 \geq 1879.8$ ppb_v was used to distinguish between air masses influenced by the monsoon ($CH_4 \geq 1879.8$ ppb_v), the SH background ($CH_4 < 1820$ ppb_v) and the NH background (1820 $ppb_v \leq CH_4 < 1879.8$ ppb_v) (Tomsche et al., 2019).

4 Results and discussion

4.1 Data processing

Data were collected from a merged data set given as 60-second-means (calculated from the original data set obtained at higher resolutions) in order to get the same time resolution for all compounds. The given time is the middle of the block mean.

For the histograms the concentrations of all species shown were binned into samples with a width of 10 ppt_v, starting the plots with the lowest bin. To compare the simulations from EMAC with measured and PSS calculated data, the corresponding values (out of the 60-second-means) were used at the given times from EMAC.

4.2 Case study: Flight 17 from Gan to Bahrain (10.08.2015)

In a case study analyzing flight 17 from 10th of august 2015, the method used to determine the origin of the measured air masses and a quantification and comparison of measured and simulated mixing ratios of H_2O_2, PSS-MHP and PSS-UHP is presented. During this flight we encountered the SH and NH as well as the monsoon in the UT. The flight track is shown in Figure 3 (dotted line). Take-off was in Gan (Maldives) and landing in Bahrain on the Arabian Peninsula. Besides take-off and landing, the entire flight took place in the UT (<230 hPa). The calculated back trajectories show the origin of the air masses. At the beginning of the flight the measured air masses had their origin over the Indian Ocean and Indonesia. During the remaining flight the measured air stemmed from India. Tomsche et al. 2019 showed that the measured air in the AMA was affected by deep convection over India resulting in methane mixing ratios above the threshold. Figure 4 shows the time series for measured H_2O_2 during the flight at the time steps given from the frequency of EMAC output (orange circles). The colored bar on top shows the origin of air masses, i.e. red for monsoon, green for NH and blue for SH. The *in situ* H_2O_2 mixing ratios vary between 128–366 ppt_v. The modelled EMAC H_2O_2 data are in the range of 110–799 ppt_v (grey triangles). For the beginning of the flight model simulations agree rather well with the measurement data. At around 6:00 UTC the model calculated mixing ratios increase to more than 500 ppt_v, while the measured data decrease to 200 ppt_v and lower. In this period a maximum difference between model and *in situ* data of 386 ppt_v was found. One hour later the EMAC model data decrease to 416 ppt_v and the *in situ* data

increase to 214 ppt_v. During the following hour until around 8:00 UTC and thus at the higher altitude, both mixing ratios increase with the modelled data showing a much stronger increase up to approximately 800 ppt_v while the *in situ* data increase only to 230 ppt_v. During the last period of the flight, simulated and measured data are again in good agreement. Here the mixing ratios from EMAC are in the range of 110–157 ppt_v while the measured data are in the range of 128–203 ppt_v. This steep drop of the modelled H_2O_2 might arise due to a change in the flight altitude, since between 8:01–8:06 UTC the aircraft changed from a flight level at 11,700 m to one aloft at 13,900 m.

In addition to EMAC simulations Figure 4 also shows the calculated PSS-H_2O_2 obtained from equation 15. Observed and PSS values for H_2O_2 mixing ratios agree very well, with a median deviation of 42 ppt_v, well within the combined uncertainties of measured data (25%) and PSS simulations (45%).

In Figure 5 the time series of *in situ* H_2O_2, PSS-MHP and PSS-UHP mixing ratios are shown (5 min means). In the beginning of the flight PSS-MHP is the dominant organic hydroperoxide. The mixing ratios are in the range of 140–341 ppt_v similar to those of *in situ* H_2O_2 (143–337 ppt_v). PSS-UHP mixing ratios are in the range of 24–162 ppt_v with a mean of 89 ppt_v. Later during the flight PSS-UHPs are the dominant hydroperoxides in air masses inside the AMA originating from India. Here we found PSS-UHP mixing ratios up to 275 ppt_v. The *in situ* H_2O_2 mixing ratios show a similar temporal pattern and mixing ratio levels to those of PSS-UHP over the Arabian Sea and the Arabian Peninsula, with values in the range of 140–243 ppt_v. PSS-MHP mixing ratios are much lower (62–130 ppt_v, median 72 ppt_v) in this area. During this part of the flight the similarity in the time series of acetone and PSS-UHP (Figure 6), indicate either similar source regions for both species, or the role of acetone as a precursor for the PSS-UHP in monsoon influenced air masses. From 6:20 UTC onwards an increase in both compounds is observed until 7:45 UTC, followed by a steep drop with a minimum at 8:17 UTC. The PSS-UHP and acetone mixing ratios in this part of the flight are strongly correlated (Figure 7), with a slope of 0.19±0.02 (ppb_v/ppb_v) and an offset of (-0.003±0.02) ppb_v. The regression coefficient R^2 is very high (0.99). For H_2O_2 and ROOH the correlation is not that strong with slopes of -0.02±0.02 (ppb_v/ppb_v) and 0.13±0.03 (ppb_v/ppb_v) respectively and offsets of (0.21±0.02) ppb_v and (0.11±0.03) ppb_v (Figure 6). The relation between ROOH mixing ratios and an air mass age tracer based on the ratio between [NO] to [NO_y] shows higher values of ROOH at smaller ratios representing older or more processed air masses (Figure 8), since highest ROOH mixing ratios (>200 ppt_v) are found at the lowest [NO]/[NO_y] ratios (all <0.19). Thus, most of the observed ROOH was measured in aged air masses transported within the anticyclone. The correlation with PSS-UHP shows that this effect is mainly due to PSS-UHP. For H_2O_2 there are also some higher mixing ratios for high [NO] to [NO_y] mixing ratios and thus fresher air (Figure 7).

4.3 Results for the entire campaign

To extend the analysis to the entire campaign, Figure 9 shows all flight tracks in the UT during OMO. The color-code represents observed mixing ratios of *in situ* H_2O_2, PSS-MHP and PSS-UHP varying from low (purple) to high values (red). Histograms for the whole campaign of observed H_2O_2 mixing ratios as well inferred PSS-MHP and PSS-UHP mixing ratios are presented in Figure 10. Here only data from the UT (<300 hPa which corresponds to altitudes >9 km) were included in the analysis. Mixing ratios for all species were further differentiated by methane levels, such that data in air masses with CH_4 mixing ratios above the threshold of 1879.8 ppb_v were classified as monsoon influenced, while air masses with a CH_4

mixing ratios between 1820 ppb_v and 1879.8 ppb_v were classified as NH background and those with CH_4 <1820 ppb_v as SH following Tomsche et al., 2019). The upper panel indicates that *in situ* H_2O_2 mixing ratios are most abundant at values of 70–90 ppt_v in NH background air masses (green), 130 ppt_v to 270 ppt_v with three notable peaks at 180–190 ppt_v, 210–220 ppt_v and 250–270 ppt_v in SH air masses (blue) and 150–170 ppt_v in AMA influenced air masses (red). The medians are 115 ppt_v for the NH background, 211 ppt_v for the SH and 167 ppt_v for the AMA, indicating an excess of 52 ppt_v in monsoon influenced air masses compared to the NH background, while in the SH the *in situ* H_2O_2 mixing ratio is twice as high as the NH background. For PSS-MHP (Figure 10, middle panel) the frequency distribution in the NH background shows a maximum at 30–40 ppt_v (green). For AMA influenced air a sharp maximum at 50–70 ppt_v (red) is found. Air masses from the SH exhibit a rather flat distribution with a maximum at values of 40–50 ppt_v and a median of 152 ppt_v (blue). With median mixing ratios of 70 ppt_v and 64 ppt_v we found only slightly higher mixing ratios for monsoon influenced air masses in comparison to the NH background. For PSS-UHP (Figure 10, bottom panel) we again found a flat distribution of mixing ratios in the SH (blue) with a maximum at values of 140–150 ppt_v and a median of 129 ppt_v. The maximum in the frequency distribution for NH background conditions is found at 70–90 ppt_v (green), while in monsoon influenced air masses it was significantly higher with 210–230 ppt_v (red). Thus, mixing ratios of PSS-UHP are approximately 2–3 times higher in the monsoon outflow than in the NH background. This is also represented in the medians of 210 ppt_v in the monsoon and 89 ppt_v in the NH background.

In the analysis of flight 17 we found a strong correlation between PSS-UHP and acetone (Figure 7) and an increase of PSS-UHP at the highest air mass ages, represented by low $[NO]/[NO_y]$ (Figure 8). Extension of this analysis to all observations in the upper troposphere obtained during OMO yields similar results for the relation between PSS-UHP, *in situ* ROOH and *in situ* H_2O_2 and acetone (Figure 11). Enhanced mixing ratios of hydroperoxides are typically associated with enhanced acetone mixing ratios, especially for PSS-UHP. A simple calculation of the production of MHP out of the photolysis of acetone and the reaction of acetaldehyde (from EMAC) with OH shows that per day appr. 40 ppt_v MHP can be formed within the AMA. The lifetime of MHP was calculated to be around 1.5 days. Thus not all of the PSS-UHP in the AMA (median 210 ppt_v) can be accounted for MHP that was chemically produced from VOCs in the AMA. The scatter plots of the hydroperoxides vs. $[NO]/[NO_y]$ for the whole data set, show no clear correlation with a large spread of hydroperoxides mixing ratios at the lowest $[NO]/[NO_y]$ ratios, representing the oldest, i.e. chemically most processed air masses (Figure 12).

4.3.1 H_2O_2 steady-state calculation

A scatter plot of the results from the H_2O_2 photostationary steady-state calculation based on observed HO_x data in the UT (eq. 15) is shown in Figure 13. The black dotted line shows the 1:1 line, the green dashed lines represent the 2:1 and 1:2 relations. It is obvious that the comparison is affected by a rather large offset of approximately 350 ppt_v in the observations that is not accounted for in the steady-state calculations. The deviations from unity in the slope are within the combined uncertainties of measured and steady-state estimations of H_2O_2 (51%, 1 σ). The regression coefficient is quite high (0.83), even though most of the calculated steady-state mixing ratios (75%) are in the range between 0 and 65 ppt_v with a median value of 15 ppt_v, while the measured mixing ratios extend over a larger range mainly between 10–210 ppt_v with a median of 150 ppt_v and thus 10 times higher than for steady-state, which

can also be seen in the histograms in Figure 14. Table 1 shows the statistical comparison of both data sets. The discrepancy between *in situ* and PSS-H_2O_2 shows that the local PSS does not account all main contributions of H_2O_2 even though all chemical reactions are included. Thus transport phenomena like deep convection seem to play a key role (see 4.3.3).

4.3.2 Comparison to EMAC

Figure 1 shows histograms for the comparison between H_2O_2, MHP and UHP observations with EMAC simulations. Hydrogen peroxide simulations from EMAC cover a broader range of mixing ratios for both NH background (6 ppt_v up to 576 ppt_v) and AMA (8–714 ppt_v) compared to observations (NH background: 20–301 ppt_v; AMA 46–446 ppt_v). For the SH model simulations and observations cover almost identical ranges of 15–409 ppt_v and 85–510 ppt_v, respectively. Median EMAC-H_2O_2 values are similar for NH background (66 ppt_v) and AMA (71 ppt_v) conditions (Table 2), while observations indicate an enhancement of +64 ppt_v in the AMA relative to the NH background. For the SH the model simulated H_2O_2 mixing ratios is four times higher than in the NH background (272 ppt_v), while the observations only show a median increase by 47 ppt_v to 211 ppt_v (Table 2).

EMAC mainly simulates MHP mixing ratios lower than 50 ppt_v for background and AMA, while PSS-MHP ranges from LOD–140 ppt_v. Again the model simulates highest MHP mixing ratios in the SH with values up to 502 ppt_v compared to up to 346 ppt_v in the PSS-MHP calculations. Similar as for H_2O_2, medians of EMAC-MHP for NH background and monsoon conditions are almost identical (11 ppt_v and 13 ppt_v respectively, Table 2) in the model simulations, while the observations show a small difference towards higher mixing ratios in the AMA (64 ppt_v and 70 ppt_v, respectively). In the simulations, southern hemispheric EMAC-MHP mixing ratios are almost ten times higher than NH background values, compared to two to three times higher in the observations.

Data for UHP in the model are calculated from the sum of simulated ethyl hydroperoxide (EHP) and peroxyacetic acid (PAA), which are the only non-methyl organic hydroperoxides in the free troposphere according to the model. EMAC-UHP mixing ratios range from 1–238 ppt_v in the NH background, 1–259 ppt_v in the AMA and 1–132 ppt_v in the SH. PSS-UHP based on the observations indicate lowest mixing ratios in the NH background (LOD–261 ppt_v), while in the AMA and the SH the ranges are quite similar (80–311 ppt_v and LOD–334 ppt_v). A comparison of median values emphasizes the large difference between model simulations and observation based estimates. In the NH background, the median PSS-UHP mixing ratio from the observations is 70 ppt_v higher than EMAC simulations (78 ppt_v and 8 ppt_v respectively). In the AMA the difference is even larger, with about 200 ppt_v higher PSS-UHP levels compared to the EMAC simulations. The smallest difference with a factor of four was found for the SH (Table 2).

4.3.3 Longitudinal gradients

So far discussions of different air masses have been based on measurements of methane, subdividing the observations in NH background, AMA and SH data. Tomsche et al., 2019) have shown that longitudinal gradients are found in the AMA over the Arabian Peninsula. Observations in the west are often near the edge of the anticyclone, while observations towards the east are closer to its center. In Figure 17 observations, steady-state calculations and EMAC simulations for upper tropospheric (9–15 km) H_2O_2 are

displayed as a function of longitude from west to east (20–30 °N, 36–60 °E, according to the red box in Figure 16). To identify gradients, the data are subdivided into bins of 2° longitude. The observations (orange) show roughly a 100% increase of *in situ* H_2O_2 from west to east (90 ppt_v to 175 ppt_v), similar to simulation with EMAC (black), although absolute mixing ratio levels in EMAC-H_2O_2 are smaller (61 ppt_v to 121 ppt_v). Contrary to these observed gradients, PSS-H_2O_2 based on HORUS data (blue) do not vary with longitude, except for the last two bins. The steady-state calculations are based exclusively on observed concentrations of HO_2 and OH radicals and thus yield only the net photochemical production, while the EMAC simulations and the observations will also account for vertical and horizontal advection from up-wind source regions. Previous studies show inconsistent results. Snow et al. (2007) and Barth et al. (2016) for example both show that H_2O_2 is depleted in convective outflow compared to background upper troposphere. In contrast, other studies found that deep convection can be a source of H_2O_2 in the upper troposphere (e.g. Jaeglé et al., 1997; Prather and Jacob, 1997; Mari et al., 2003; Bozem et al., 2017). Similarly, convection over India during the summer monsoon is a potential source of excess H_2O_2 in the upper troposphere. With a photochemical lifetime of several days, this excess in H_2O_2 reaches the western AMA, giving rise to the observed and model simulated longitudinal gradients. Since the steady-state calculations do not account for transport this can explain the rather large deviation of 150 ppt_v with the observations. Differences between observation and EMAC simulation could potentially arise due to uncertainties in the scavenging efficiency for H_2O_2, as the chemistry does not seem to be a dominant cause of uncertainty.

Similar longitudinal gradients are also observed for measured total organic hydroperoxides (ROOH, green asterisks in Figure 18), inferred PSS-UHP (black) as well as total ROOH in EMAC (blue). Steady-state calculations of MHP (pink) and EMAC simulations of MHP (yellow) show either no, or only weak longitudinal gradients. Assuming that MHP is also enhanced in the outflow of deep convection at least part of the enhancement in ROOH (and thus inferred PSS-UHP) could be due to advected MHP.

4.4 Discussion

To our knowledge we present the first observations of H_2O_2 and ROOH mixing ratios in the Asian Monsoon Anticyclone. Previous studies have been mainly focused on the northern hemispheric upper troposphere. Several aircraft campaigns including peroxide measurements were performed over North America. They are summarized in Snow et al., 2007): The SONEX campaign took place in fall 1997 in the UT and yielded mean values of 120 ppt_v for H_2O_2 and 50 ppt_v for MHP (medians: 80 ppt_v and 30 ppt_v, respectively). The TOPSE campaign in winter/spring 2000 probed the middle troposphere yielding median H_2O_2 and MHP mixing ratios of 150 ppt_v for both species. During the INTEX-NA campaign in summer 2004 observed median mixing ratios at altitudes of 6–10 km were about 400 ppt_v for H_2O_2, and 200 ppt_v for MHP. A comparison with our results (Table 2) shows that we found similar mixing ratios as in SONEX in the northern hemispheric background of 115 ppt_v and 64 ppt_v for H_2O_2 and MHP, respectively. Mixing ratios for both species reported for TOPSE and INTEX-NA are slightly higher than ours, which may be related to the lower altitude range of 6–10 km (in comparison to >9 km for OMO) in these studies. Previous observations have shown that H_2O_2 and MHP show highest mixing ratios at altitudes between 2–5 km followed by a sharp decrease towards higher altitudes (see e.g. Daum et al., 1990; Heikes, 1992; Weinstein-Lloyd et al., 1998; Snow, 2003; Snow et al., 2007; Klippel et al., 2011).

Heikes et al. associated enhanced H_2O_2 mixing ratios above 5 km in the North Pacific of the Asian coast (30 °N) with outflow from the typhoon Mireille (Heikes et al., 1996). These observations were made close to the source region for the monsoon influenced air masses described here (see back trajectories in the case study of flight 17, Figure 3 or Tomsche et al., 2019). For MHP Heikes et al. (1996) found mixing ratios of 250–500 ppt_v in the southern longitudinal section above 5 km, similar to median mixing ratios of 152 ppt_v for MHP in SH air masses in the UT found in this study.

Although the mixing ratios observed during this study are similar to previous observations in the upper troposphere, one striking result is that a state-of-the-art global circulation model (EMAC) and a local steady-state calculation constrained by measured radical levels significantly underestimate H_2O_2 mixing ratios in particular in the AMA. The general tendency is that the steady-state model produces the lowest values, with EMAC falling in between steady-state and observations (e.g. Figure 17). A comparison of the EMAC simulations for the two radicals that affect H_2O_2 most strongly (OH and HO_2) yields a rather good agreement. A scatter plot between modelled and *in situ* HO_2 yields a slope of 0.72±0.01 (ppt_v/ppt_v) and an offset of (4.30±0.09) ppt_v with a regression coefficient R^2 of 0.89 (Figure 19 left). The OH data show more scatter with a tendency for EMAC to overestimate the mixing ratios (slope: 1.7±0.2 (ppt_v/ppt_v); offset: (-0.1±0.1) ppt_v; regression coefficient: 0.67, Figure 19 right). Although there is rather good agreement between EMAC simulations and observations for all the species that affect the local photochemical budget of H_2O_2, EMAC significantly exceeds PSS calculation for H_2O_2. This is an indication that an additional H_2O_2 source is accounted for in the global model and that the local photo-stationary-state assumption is not fulfilled. The additional source is attributed to transport associated with deep convection over India, yielding in an upwind source of H_2O_2 that is significant throughout the western part of the AMA. In the AMA, clouds are absent, so that gas phase photochemical processes may determine the lifetime of H_2O_2. Based on observed OH levels and photolysis frequencies during OMO the H_2O_2 lifetime in the upper troposphere is of the order of several days, sufficiently long for the excess H_2O_2 to reach the western parts of the AMA, producing the observed longitudinal H_2O_2 gradient observed in both observations and EMAC simulations (Figure 17). The total amount of H_2O_2 injected into the UT by convective outflow depends on the scavenging efficiency (Mari et al., 2000; Barth et al., 2016; Bozem et al., 2017). Differences between H_2O_2 observations and EMAC simulations are most likely due to an overestimation of scavenging in the model as also pointed out by Klippel et al., 2011). To investigate this assumption we performed a sensitivity study with EMAC excluding scavenging. The result is shown in Figure 20. The H_2O_2 mixing ratios significantly increase with longitude by a factor of 3–4 and thus to the level of observed H_2O_2.

There is a rather large uncertainty regarding the scavenging efficiency of MHP in deep convection (Barth et al., 2016). For the Trace A campaign Mari et al., 2000) found observed (modelled) enhancement ratios of postconvective to preconvective mixing ratios of 11 (9.5) for MHP and 1.9 (1.2) for H_2O_2. Such efficient transport in the Indian Summer Monsoon would yield a strong source of upper tropospheric MHP explaining the large enhancement of ROOH in the AMA described here. It seems that a large part of the PSS-UHP is actually MHP advected throughout the AMA after deep convective transport over India. In the EMAC simulations the transport of MHP is less efficient and thus EMAC-MHP is lower than PSS-MHP and PSS-UHP.

5 Conclusion

Hydrogen peroxide and organic hydroperoxides were measured during the OMO campaign in the upper troposphere in NH background air over the western Mediterranean, the Asian Summer Monsoon Anticyclone over the Arabian Peninsula and the SH over the Maldives and the Indian Ocean in summer 2015. The observed mixing ratios for background conditions in the NH and SH are in line with previous studies described in the literature. A case study (of flight 17) revealed enhanced H_2O_2 and ROOH mixing ratios in the AMA relative to the NH background. Similar results are found for other flights throughout the campaign. The atmospheric chemistry-general circulation model EMAC slightly underestimates H2O2 in the NH background (medians: 66 pptv vs. 100 pptv), significantly underestimates it in the AMA (medians: 71 pptv vs. 164 pptv), and overestimates it in the SH (medians: 272 pptv vs. 211 pptv). Steady-state calculations for H2O2 and MHP based on observed precursors yield much lower values, in particular in the AMA, resulting in a large contribution of an unidentified organic hydroperoxide (UHP) in air masses affected by the Asian summer monsoon. A comparison between EMAC simulations and HO_x levels shows a good agreement indicating that deviations between simulated and steady-state H_2O_2 levels are due to transport. Convective injection of H_2O_2 (and MHP) into the upper troposphere over India most likely forms a pool of hydroperoxides in the upper troposphere that subsequently influences the western AMA, giving rise to a significant longitudinal gradient of H_2O_2 and MHP mixing ratios, with increasing values towards the center of the AMA. It is likely that at least a large part of UHP is due to additional MHP from an up-wind source.

Data availability

The data are available from the HALO database (https://halo-db.pa.op.dlr.de/, last access: 7 November 2019).

Author contributions

BH and SH were responsible for H_2O_2 and ROOH measurements and data. BH conducted further data analysis and wrote the original draft of the paper in close cooperation with HF. CH_4 and CO data were provided by LT, HO_x data by DM, MM and HH, O_3 and acetone data by MN and AZ, photolysis frequencies by BB and NO and NO_y data by HZ and GS. AP was responsible for the EMAC model simulations. JL was the principal investigator of the OMO mission. All authors were involved in the review and editing of the paper.

Competing interests

The authors declare that they have no conflict of interest.

Acknowledgements

We would like to thank all of the participants of the OMO mission, the German Aerospace Center (DLR), and EDT Offshore Ltd in Cyprus for their cooperation during the mission. We further thank Rainer Königstedt for installing the TRIHOP instrument and Uwe Parchatka for supporting the measurements of CO and CH_4.

References

AEROLASER: AL2021 H_2O_2-Monitor User Manual, Version 2.20, Rev.02, Garmisch-Partenkirchen, Germany, 2006.

Atkinson, R., Baulch, D. L., Cox, R. A., Crowley, J. N., Hampson, R. F., Hynes, R. G., Jenkin, M. E., Rossi, M. J., and Troe, J.: Evaluated kinetic and photochemical data for atmospheric chemistry: Volume I – gas phase reactions of O_x, HO_x, NO_x and SO_x species, Atmos. Chem. Phys., 4, 1461–1738, doi:10.5194/acp-4-1461-2004, 2004.

Atkinson, R., Baulch, D. L., Cox, R. A., Crowley, J. N., Hampson, R. F., Hynes, R. G., Jenkin, M. E., Rossi, M. J., Troe, J., and IUPAC Subcommittee: Evaluated kinetic and photochemical data for atmospheric chemistry: Volume II – gas phase reactions of organic species, Atmos. Chem. Phys., 6, 3625–4055, doi:10.5194/acp-6-3625-2006, 2006.

Barret, B., Sauvage, B., Bennouna, Y., and Le Flochmoen, E.: Upper-tropospheric CO and O_3 budget during the Asian summer monsoon, Atmos. Chem. Phys., 16, 9129–9147, doi:10.5194/acp-16-9129-2016, 2016.

Barth, M. C., Bela, M. M., Fried, A., Wennberg, P. O., Crounse, J. D., St. Clair, J. M., Blake, N. J., Blake, D. R., Homeyer, C. R., Brune, W. H., Zhang, L., Mao, J., Ren, X., Ryerson, T. B., Pollack, I. B., Peischl, J., Cohen, R. C., Nault, B. A., Huey, L. G., Liu, X., and Cantrell, C. A.: Convective transport and scavenging of peroxides by thunderstorms observed over the central U.S. during DC3, J. Geophys. Res. Atmos., 121, 4272–4295, doi:10.1002/2015JD024570, 2016.

Bohn, B. and Lohse, I.: Calibration and evaluation of CCD spectroradiometers for ground-based and airborne measurements of spectral actinic flux densities, Atmos. Meas. Tech., 10, 3151–3174, doi:10.5194/amt-10-3151-2017, 2017.

Bozem, H., Pozzer, A., Harder, H., Martinez, M., Williams, J., Lelieveld, J., and Fischer, H.: The influence of deep convection on HCHO and H_2O_2 in the upper troposphere over Europe, Atmos. Chem. Phys., 17, 11835–11848, doi:10.5194/acp-17-11835-2017, 2017.

Burkholder, J. B., Sander S. P., Abbatt J., Barker J. R., Huie R. E., Kolb C. E., Kurylo M. J., Orkin V. L., and Wilmouth D. M. and Wine P. H.: Chemical Kinetics and Photochemical Data for Use in Atmospheric Studies, JPL Publication 15-10, Jet Propulsion Laboratory, Pasadena, 2015.

Calvert, J. G., Lazrus, A., Kok, G. L., Heikes, B. G., Walega, J. G., Lind, J., and Cantrell, C. A.: Chemical mechanisms of acid generation in the troposphere, Nature, 317, 27–35, doi:10.1038/317027a0, 1985.

Crutzen, P. J., Lawrence, M. G., and Pöschl, U.: On the background photochemistry of tropospheric ozone, Tellus B: Chemical and Physical Meteorology, 51, 123–146, doi:10.3402/tellusb.v51i1.16264, 1999.

Daum, P. H., Kleinman, L. I., Hills, A. J., Lazrus, A. L., Leslie, A. C. D., Busness, K., and Boatman, J.: Measurement and interpretation of concentrations of H_2O_2 and related species in the upper midwest during summer, J. Geophys. Res., 95, 9857–9871, doi:10.1029/JD095iD07p09857, 1990.

Emanuel K. A. and Zivkovic-Rothman M.: Development and Evaluation of a Convection Scheme for Use in Climate Models, Journal of Atmospheric Sciences, 1766–1782, doi:10.1175/1520-0469(1999)056<1766:DAEOAC>2.0.CO;2, 1999.

Faloona, I., Tan, D., Brune, W. H., Jaeglé, L., Jacob, D. J., Kondo, Y., Koike, M., Chatfield, R., Pueschel, R., Ferry, G., Sachse, G., Vay, S., Anderson, B., Hannon, J., and Fuelberg, H.: Observations of HO_x and its relationship with NO_x in the upper troposphere during SONEX, J. Geophys. Res., 105, 3771–3783, doi:10.1029/1999JD900914, 2000.

Faloona, I. C., Tan, D., Lesher, R. L., Hazen, N. L., Frame, C. L., Simpas, J. B., Harder, H., Martinez, M., Di Carlo, P., Ren, X., and Brune, W. H.: A Laser-induced Fluorescence Instrument for Detecting Tropospheric OH and HO_2: Characteristics and Calibration, Journal of Atmospheric Chemistry, 47, 139–167, doi:10.1023/B:JOCH.0000021036.53185.0e, 2004.

Gettelman, A., Kinnison, D. E., Dunkerton, T. J., and Brasseur, G. P.: Impact of monsoon circulations on the upper troposphere and lower stratosphere, J. Geophys. Res., 109, n/a-n/a, doi:10.1029/2004JD004878, 2004.

Heikes, B. G.: Formaldehyde and hydroperoxides at Mauna Loa Observatory, J. Geophys. Res., 97, 18001, doi:10.1029/92JD00268, 1992.

Heikes, B. G., Lee, M., Bradshaw, J., Sandholm, S., Davis, D. D., Crawford, J., Rodriguez, J., Liu, S., McKeen, S., Thornton, D., Bandy, A., Gregory, G., Talbot, R., and Blake, D.: Hydrogen peroxide and methylhydroperoxide distributions related to ozone and odd hydrogen over the North Pacific in the fall of 1991, J. Geophys. Res., 101, 1891–1905, doi:10.1029/95JD01364, 1996.

Hoffmann, M. R. and Edwards, J. O.: Kinetics of the oxidation of sulfite by hydrogen peroxide in acidic solution, J. Phys. Chem., 79, 2096–2098, doi:10.1021/j100587a005, 1975.

Jackson, A. V. and Hewitt, C. N.: Hydrogen peroxide and organic hydroperoxide concentrations in air in a eucalyptus forest in central Portugal, Atmospheric Environment, 30, 819–830, doi:10.1016/1352-2310(95)00348-7, 1996.

Jacob, P. and Klockow, D.: Hydrogen peroxide measurements in the marine atmosphere, J Atmos Chem, 15, 353–360, doi:10.1007/BF00115404, 1992.

Jaeglé, L., Jacob, D. J., Brune, W. H., Faloona, I., Tan, D., Heikes, B. G., Kondo, Y., Sachse, G. W., Anderson, B., Gregory, G. L., Singh, H. B., Pueschel, R., Ferry, G., Blake, D. R., and Shetter, R. E.: Photochemistry of HO_x in the upper troposphere at northern midlatitudes, J. Geophys. Res., 105, 3877–3892, doi:10.1029/1999JD901016, 2000.

Jaeglé, L., Jacob, D. J., Wennberg, P. O., Spivakovsky, C. M., Hanisco, T. F., Lanzendorf, E. J., Hintsa, E. J., Fahey, D. W., Keim, E. R., Proffitt, M. H., Atlas, E. L., Flocke, F., Schauffler, S., McElroy, C. T., Midwinter, C., Pfister, L., and Wilson, J. C.: Observed OH and HO_2 in the upper troposphere suggest a major source from convective injection of peroxides, Geophys. Res. Lett., 24, 3181–3184, doi:10.1029/97GL03004, 1997.

Jöckel, P., Tost, H., Pozzer, A., Kunze, M., Kirner, O., Brenninkmeijer, C. A. M., Brinkop, S., Cai, D. S., Dyroff, C., Eckstein, J., Frank, F., Garny, H., Gottschaldt, K.-D., Graf, P., Grewe, V., Kerkweg, A., Kern, B., Matthes, S., Mertens, M., Meul, S., Neumaier, M., Nützel, M., Oberländer-Hayn, S., Ruhnke, R., Runde, T., Sander, R., Scharffe, D., and Zahn, A.: Earth System Chemistry integrated Modelling

(ESCiMo) with the Modular Earth Submodel System (MESSy) version 2.51, Geosci. Model Dev., 9, 1153–1200, doi:10.5194/gmd-9-1153-2016, 2016.

Klippel, T., Fischer, H., Bozem, H., Lawrence, M. G., Butler, T., Jöckel, P., Tost, H., Martinez, M., Harder, H., Regelin, E., Sander, R., Schiller, C. L., Stickler, A., and Lelieveld, J.: Distribution of hydrogen peroxide and formaldehyde over Central Europe during the HOOVER project, Atmos. Chem. Phys., 11, 4391–4410, doi:10.5194/acp-11-4391-2011, 2011.

Lawrence, M. G. and Lelieveld, J.: Atmospheric pollutant outflow from southern Asia: A review, Atmos. Chem. Phys., 10, 11017–11096, doi:10.5194/acp-10-11017-2010, 2010.

Lazrus, A. L., Kok, G. L., Gitlin, S. N., Lind, J. A., and McLaren, S. E.: Automated fluorimetric method for hydrogen peroxide in atmospheric precipitation, Anal. Chem., 57, 917–922, doi:10.1021/ac00281a031, 1985.

Lazrus, A. L., Kok, G. L., Lind, J. A., Gitlin, S. N., Heikes, B. G., and Shetter, R. E.: Automated fluorometric method for hydrogen peroxide in air, Anal. Chem., 58, 594–597, doi:10.1021/ac00294a024, 1986.

Lee, M., Heikes, B. G., and O'Sullivan, D. W.: Hydrogen peroxide and organic hydroperoxide in the troposphere: A review, Atmospheric Environment, 34, 3475–3494, doi:10.1016/S1352-2310(99)00432-X, 2000.

Lelieveld, J., Berresheim, H., Borrmann, S., Crutzen, P. J., Dentener, F. J., Fischer, H., Feichter, J., Flatau, P. J., Heland, J., Holzinger, R., Korrmann, R., Lawrence, M. G., Levin, Z., Markowicz, K. M., Mihalopoulos, N., Minikin, A., Ramanathan, V., Reus, M. de, Roelofs, G. J., Scheeren, H. A., Sciare, J., Schlager, H., Schultz, M., Siegmund, P., Steil, B., Stephanou, E. G., Stier, P., Traub, M., Warneke, C., Williams, J., and Ziereis, H.: Global air pollution crossroads over the Mediterranean, Science (New York, N.Y.), 298, 794–799, doi:10.1126/science.1075457, 2002.

Lelieveld, J., Bourtsoukidis, E., Brühl, C., Fischer, H., Fuchs, H., Harder, H., Hofzumahaus, A., Holland, F., Marno, D., Neumaier, M., Pozzer, A., Schlager, H., Williams, J., Zahn, A., and Ziereis, H.: The South Asian monsoon-pollution pump and purifier, Science (New York, N.Y.), 361, 270–273, doi:10.1126/science.aar2501, 2018.

Lelieveld, J. and Crutzen, P. J.: Influences of cloud photochemical processes on tropospheric ozone, Nature, 343, 227–233, doi:10.1038/343227a0, 1990.

Levy, H.: Normal atmosphere: large radical and formaldehyde concentrations predicted, Science (New York, N.Y.), 173, 141–143, doi:10.1126/science.173.3992.141, 1971.

Lind, J. A. and Kok, G. L.: Henry's law determinations for aqueous solutions of hydrogen peroxide, methylhydroperoxide, and peroxyacetic acid, J. Geophys. Res., 91, 7889–7895, doi:10.1029/JD091iD07p07889, 1986.

Lind, J. A. and Kok, G. L.: Correction to “Henry's law determinations for aqueous solutions of hydrogen peroxide, methylhydroperoxide, and peroxyacetic acid”, J. Geophys. Res., 99, 21119, doi:10.1029/94JD01155, 1994.

Mari, C., Jacob, D. J., and Bechtold, P.: Transport and scavenging of soluble gases in a deep convective cloud, J. Geophys. Res., 105, 22255–22267, doi:10.1029/2000JD900211, 2000.

Mari, C., Saüt, C., Jacob, D. J., Staudt, A., Avery, M. A., Brune, W. H., Faloona, I., Heikes, B. G., Sachse, G. W., Sandholm, S. T., Singh, H. B., and Tan, D.: On the relative role of convection, chemistry, and transport over the South Pacific Convergence Zone during PEM-Tropics B: A case study, J. Geophys. Res., 108, 401, doi:10.1029/2001JD001466, 2003.

Martinez, M., Harder, H., Kubistin, D., Rudolf, M., Bozem, H., Eerdekens, G., Fischer, H., Klüpfel, T., Gurk, C., Königstedt, R., Parchatka, U., Schiller, C. L., Stickler, A., Williams, J., and Lelieveld, J.: Hydroxyl radicals in the tropical troposphere over the Suriname rainforest: Airborne measurements, Atmos. Chem. Phys., 10, 3759–3773, doi:10.5194/acp-10-3759-2010, 2010.

Nunnermacker, L. J., Weinstein-Lloyd, J. B., Hillery, B., Giebel, B., Kleinman, L. I., Springston, S. R., Daum, P. H., Gaffney, J., Marley, N., and Huey, G.: Aircraft and ground-based measurements of hydroperoxides during the 2006 MILAGRO field campaign, Atmos. Chem. Phys., 8, 7619–7636, doi:10.5194/acp-8-7619-2008, 2008.

Ojha, N., Pozzer, A., Rauthe-Schöch, A., Baker, A. K., Yoon, J., Brenninkmeijer, C. A. M., and Lelieveld, J.: Ozone and carbon monoxide over India during the summer monsoon: Regional emissions and transport, Atmos. Chem. Phys., 16, 3013–3032, doi:10.5194/acp-16-3013-2016, 2016.

Penkett, S. A., Jones, B., Brich, K. A., and Eggleton, A.: The importance of atmospheric ozone and hydrogen peroxide in oxidising sulphur dioxide in cloud and rainwater, Atmospheric Environment (1967), 13, 123–137, doi:10.1016/0004-6981(79)90251-8, 1979.

Perros, P.: Large-scale distribution of hydrogen peroxide from aircraft measurements during the TROPOZ II experiment, Atmospheric Environment. Part A. General Topics, 27, 1695–1708, doi:10.1016/0960-1686(93)90232-N, 1993.

Pilz, W. and Johann, I.: Die Bestimmung Kleinster Mengen von Wasserstoffperoxyd in Luft, International journal of environmental analytical chemistry, 3, 257–270, doi:10.1080/03067317408071087, 1974.

Prather, M. J. and Jacob, D. J.: A persistent imbalance in HO_x and NO_x photochemistry of the upper troposphere driven by deep tropical convection, Geophys. Res. Lett., 24, 3189–3192, doi:10.1029/97GL03027, 1997.

Randel, W. J., Park, M., Emmons, L., Kinnison, D., Bernath, P., Walker, K. A., Boone, C., and Pumphrey, H.: Asian monsoon transport of pollution to the stratosphere, Science (New York, N.Y.), 328, 611–613, doi:10.1126/science.1182274, 2010.

Rauthe-Schöch, A., Baker, A. K., Schuck, T. J., Brenninkmeijer, C. A. M., Zahn, A., Hermann, M., Stratmann, G., Ziereis, H., van Velthoven, Peter F. J., and Lelieveld, J.: Trapping, chemistry, and export of trace gases in the South Asian summer monsoon observed during CARIBIC flights in 2008, Atmos. Chem. Phys., 16, 3609–3629, doi:10.5194/acp-16-3609-2016, 2016.

Robbin Martin, L. and Damschen, D. E.: Aqueous oxidation of sulfur dioxide by hydrogen peroxide at low pH, Atmospheric Environment (1967), 15, 1615–1621, doi:10.1016/0004-6981(81)90146-3, 1981.

Roeckner, E., Brokopf, R., Esch, M., Giorgetta, M., Hagemann, S., Kornblueh, L., Manzini, E., Schlese, U., and Schulzweida, U.: Sensitivity of Simulated Climate to Horizontal and Vertical Resolution in the ECHAM5 Atmosphere Model, J. Climate, 19, 3771–3791, doi:10.1175/JCLI3824.1, 2006.

Schiller, C. L., Bozem, H., Gurk, C., Parchatka, U., Königstedt, R., Harris, G. W., Lelieveld, J., and Fischer, H.: Applications of quantum cascade lasers for sensitive trace gas measurements of CO, CH_4, N_2O and HCHO, Appl. Phys. B, 92, 419–430, doi:10.1007/s00340-008-3125-0, 2008.

Slemr, F. and Tremmel, H. G.: Hydroperoxides in the marine troposphere over the Atlantic Ocean, J Atmos Chem, 19, 371–404, doi:10.1007/BF00694493, 1994.

Snow, J. A.: Winter-spring evolution and variability of HO_x reservoir species, hydrogen peroxide, and methyl hydroperoxide, in the northern middle to high latitudes, J. Geophys. Res., 108, 1890, doi:10.1029/2002JD002172, 2003.

Snow, J. A., Heikes, B. G., Shen, H., O'Sullivan, D. W., Fried, A., and Walega, J.: Hydrogen peroxide, methyl hydroperoxide, and formaldehyde over North America and the North Atlantic, J. Geophys. Res., 112, 8353, doi:10.1029/2006JD007746, 2007.

Stohl, A., Forster, C., Frank, A., and Seibert, P. and Wotawa, G.: Technical note: The Lagrangian particle dispersion model FLEXPART version 6.2, Atmos. Chem. Phys., 2461–2474, doi:10.5194/acp-5-2461-2005, 2005.

Stratmann, G., Ziereis, H., Stock, P., Brenninkmeijer, C., Zahn, A., Rauthe-Schöch, A., Velthoven, P. V., Schlager, H., and Volz-Thomas, A.: NO and NO_y in the upper troposphere: Nine years of CARIBIC measurements onboard a passenger aircraft, Atmospheric Environment, 133, 93–111, doi:10.1016/j.atmosenv.2016.02.035, 2016.

Tadic, I., Parchatka, U., Königstedt, R., and Fischer, H.: In-flight stability of quantum cascade laser-based infrared absorption spectroscopy measurements of atmospheric carbon monoxide, Appl. Phys. B, 123, 805, doi:10.1007/s00340-017-6721-z, 2017.

Tomsche, L., Pozzer, A., Ojha, N., Parchatka, U., Lelieveld, J., and Fischer, H.: Upper tropospheric CH_4 and CO affected by the South Asian summer monsoon during the Oxidation Mechanism Observations mission, Atmos. Chem. Phys., 19, 1915–1939, doi:10.5194/acp-19-1915-2019, 2019.

Weinstein-Lloyd, J. B., Lee, J. H., Daum, P. H., Kleinman, L. I., Nunnermacker, L. J., Springston, S. R., and Newman, L.: Measurements of peroxides and related species during the 1995 summer intensive of the Southern Oxidants Study in Nashville, Tennessee, J. Geophys. Res., 103, 22361–22373, doi:10.1029/98JD01636, 1998.

Zahn, A., Weppner, J., Widmann, H., Schlote-Holubek, K., Burger, B., Kühner, T., and Franke, H.: A fast and precise chemiluminescence ozone detector for eddy flux and airborne application, Atmos. Meas. Tech., 5, 363–375, doi:10.5194/amt-5-363-2012, 2012.

Ziereis, H., Schlager, H., Schulte, P., van Velthoven, P. F. J., and Slemr, F.: Distributions of NO, NO_x and NO_y in the upper troposphere and lower stratosphere between 28° and 61°N during POLINAT 2, J. Geophys. Res., 105, 3653–3664, doi:10.1029/1999JD900870, 2000.

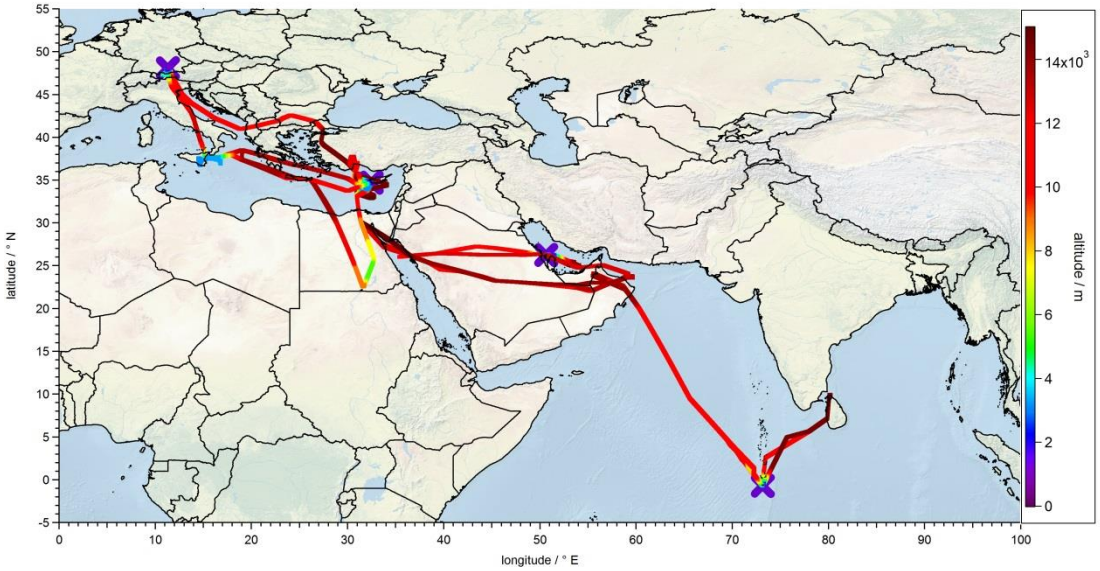

Figure 2: Flight tracks (colors indicate altitude) and airports (purple crosses) used during the OMO campaign.

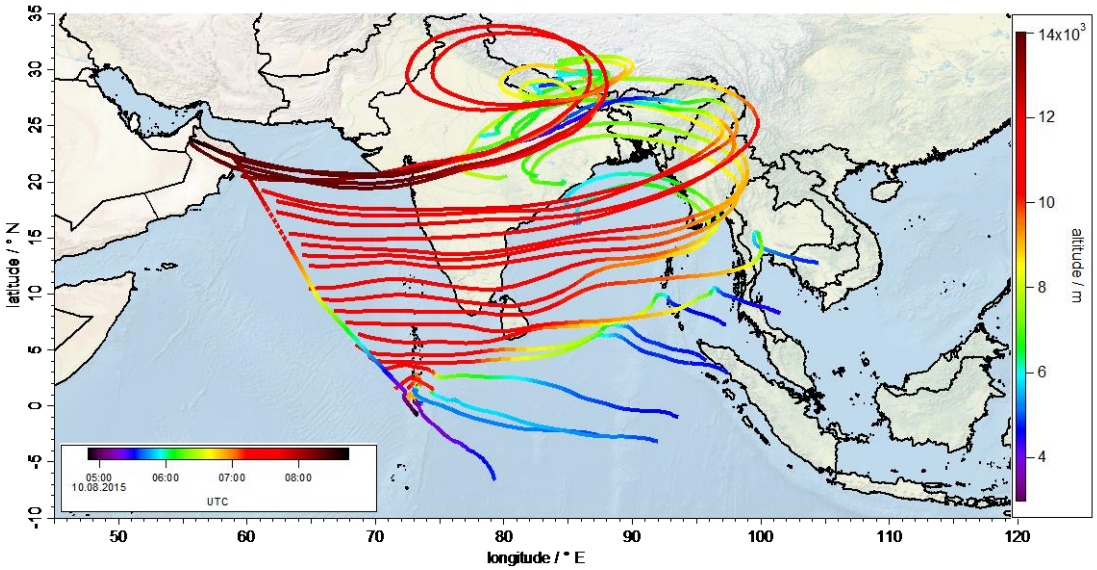

Figure 3: Track of flight 17 (black dotted line) and calculated 10-day-back trajectories (lines colored as a function of altitude) to show the origin of sampled air masses during the flight.

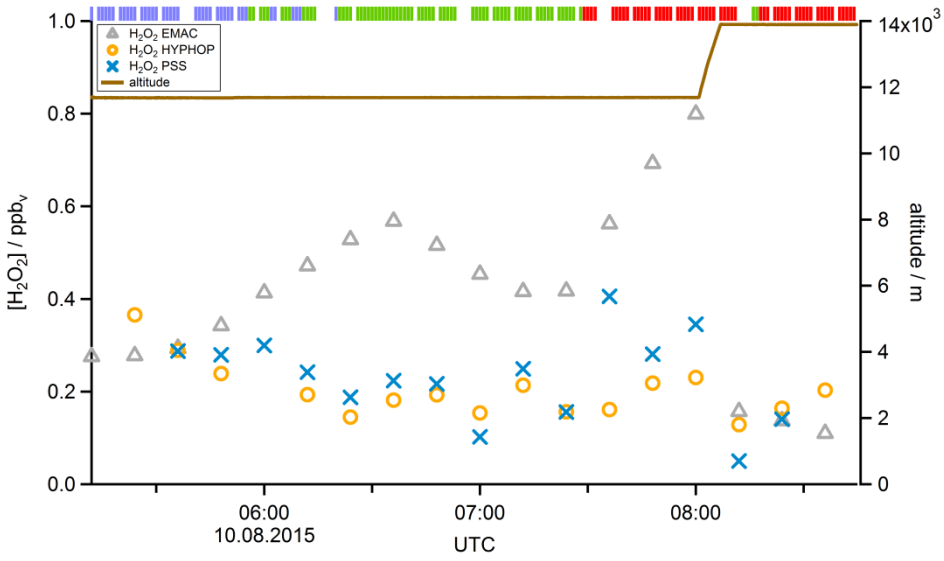

Figure 4: Time series of measured (orange circles), PSS calculated (blue crosses) and modelled (grey triangles) H_2O_2 mixing ratios for flight 17. The brown line shows the altitude, the colored bar on top indicates the origin of air masses according to the methane mixing ratio classification: for SH blue, NH green and monsoon red.

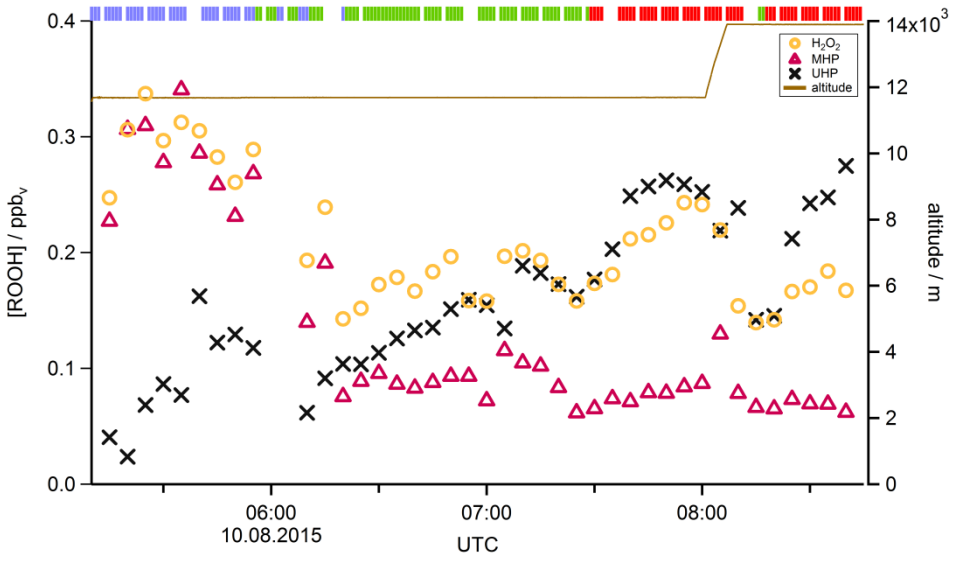

Figure 5: Time series of hydroperoxide mixing ratios during flight 17. The mixing ratios of *in situ* H_2O_2 (orange circles), PSS-MHP (purple triangles) and PSS-UHP (black crosses) are shown. The brown line shows the altitude, the colored bar on top indicates the origin of air masses according to the methane mixing ratio classification: for SH blue, NH green and monsoon red.

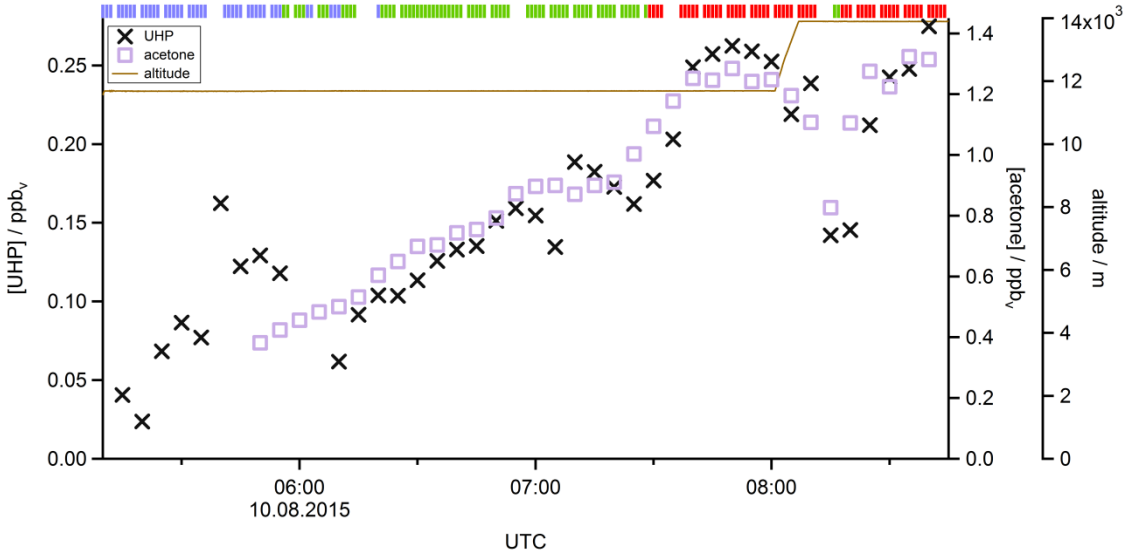

Figure 6: Time series of PSS-UHP (black crosses) and *in situ* acetone (green circles) mixing ratios during flight 17. The brown line shows the altitude, the colored bar on top indicates the origin of air masses according to the methane mixing ratio classification: for SH blue, NH green and monsoon red.

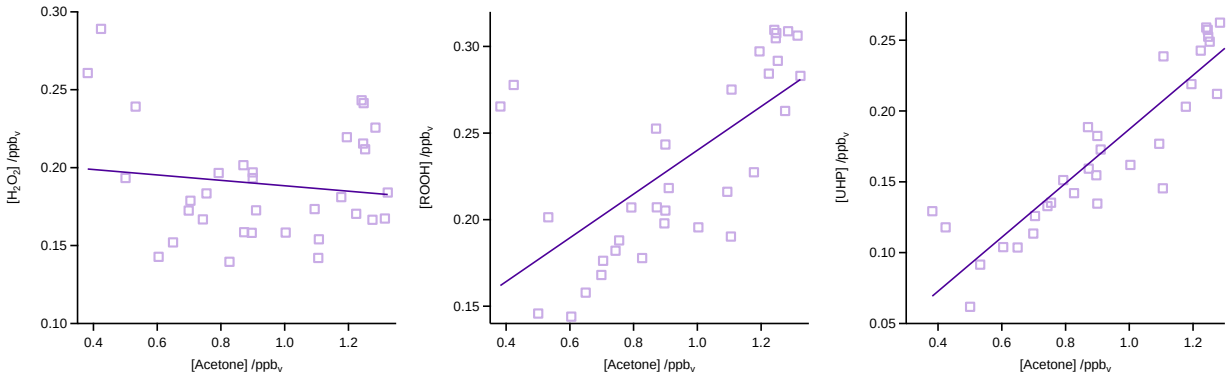

Figure 7: Scatter plots of measured acetone and *in situ* H_2O_2 (left), *in situ* ROOH (middle) and PSS-UHP (right) during flight 17. The black lines represent the least orthogonal distance fits with regression coefficients of 0.99, 0.98 and 0.99.

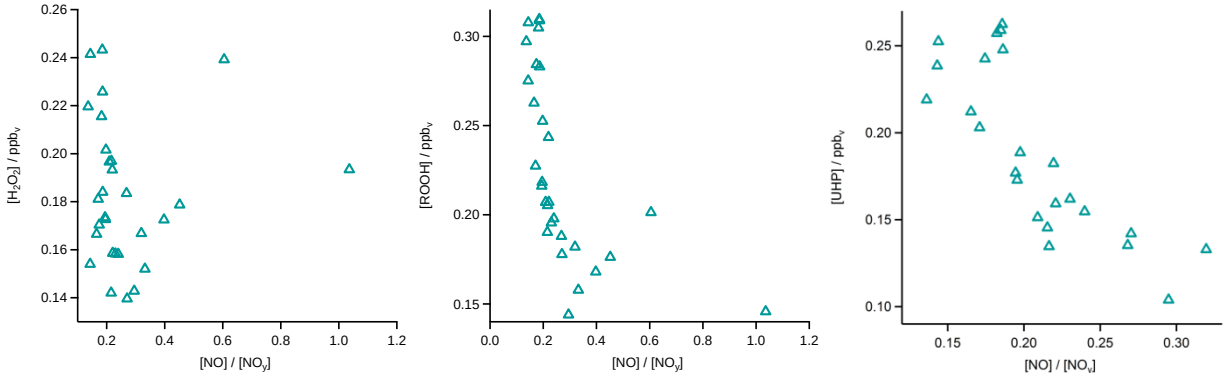

Figure 8: Scatter plots of *in situ* H_2O_2 (left), *in situ* ROOH (middle) and PSS-UHP (right) and NO/NO_y ratio during flight 17.

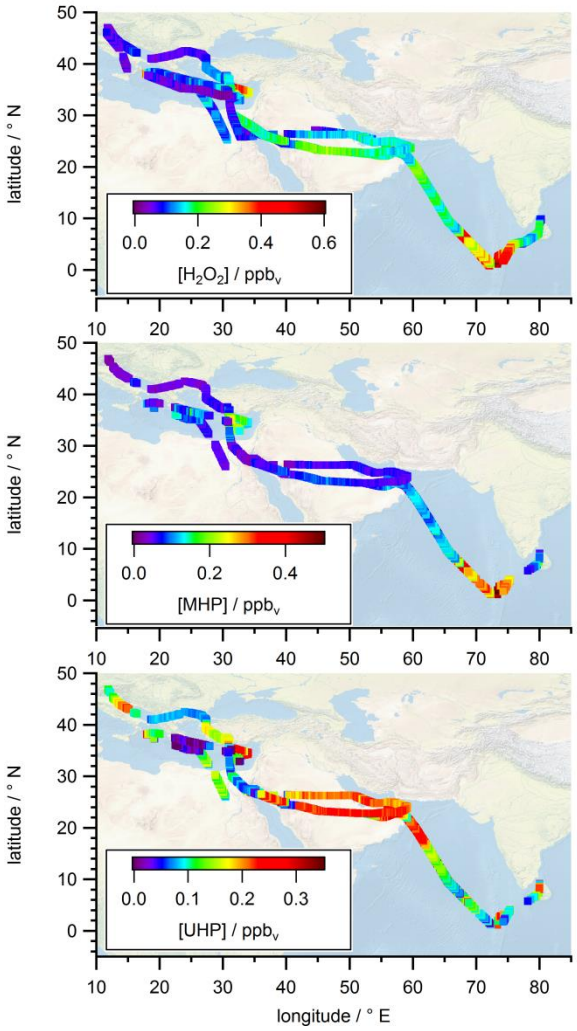

Figure 9: All flight positions in the upper troposphere (p<300 hPa) during OMO as a function of (a) in situ H_2O_2 on top, (b) PSS-MHP in the middle and (c) PSS-UHP at the bottom.

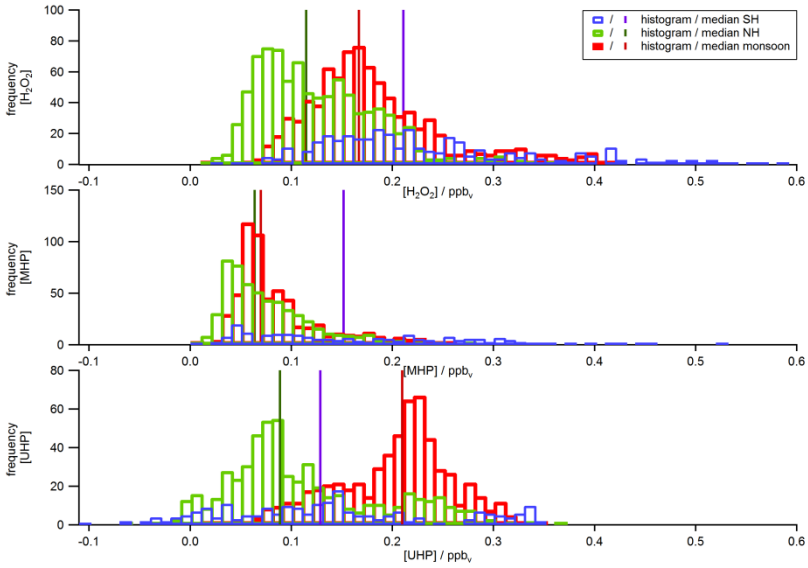

Figure 10: Histograms of *in situ* H_2O_2 (top), PSS-MHP (middle) and PSS-UHP (bottom) mixing ratios during the OMO campaign for NH background (green), SH (blue) and monsoon (red) air masses.

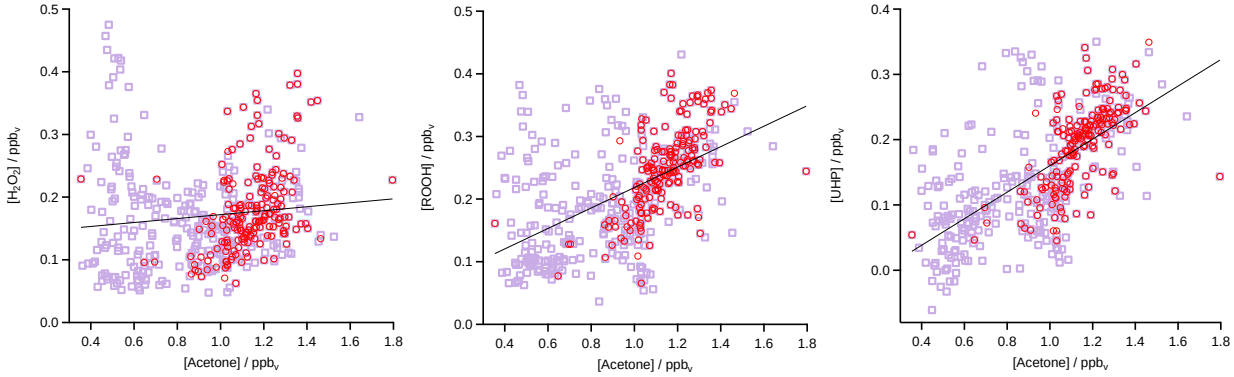

Figure 11: Scatter plots of *in situ* acetone and *in situ* H_2O_2 (left), *in situ* ROOH (middle) and PSS-UHP (right) in the UT (purple squares) and especially in the AMA (red circles). The black lines represent the least orthogonal distance fit with linear regression coefficients of 0.96 (H_2O_2), 0.97 (ROOH) and 0.96 (UHP).

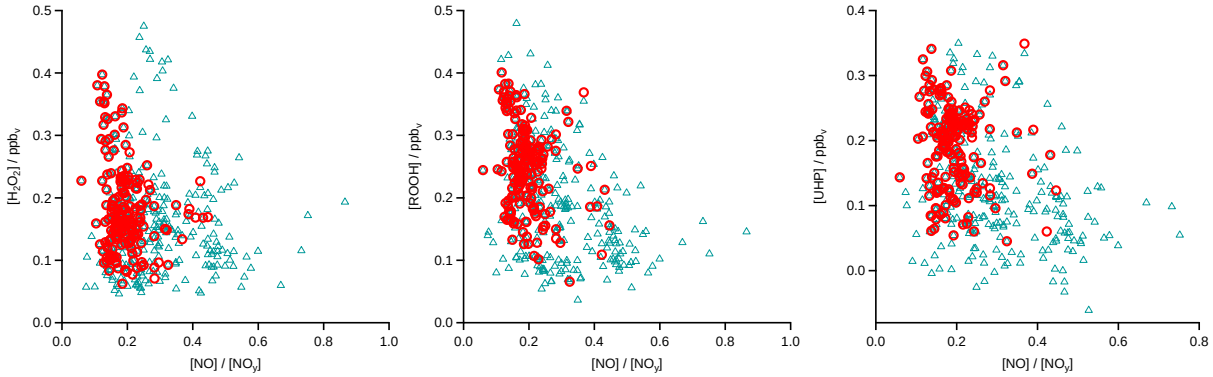

Figure 12: Scatter plots of NO/NO_y and *in situ* H_2O_2 (left), *in situ* ROOH (middle) and PSS-UHP (right) in the UT (blue triangles) and especially in the AMA (red circles).

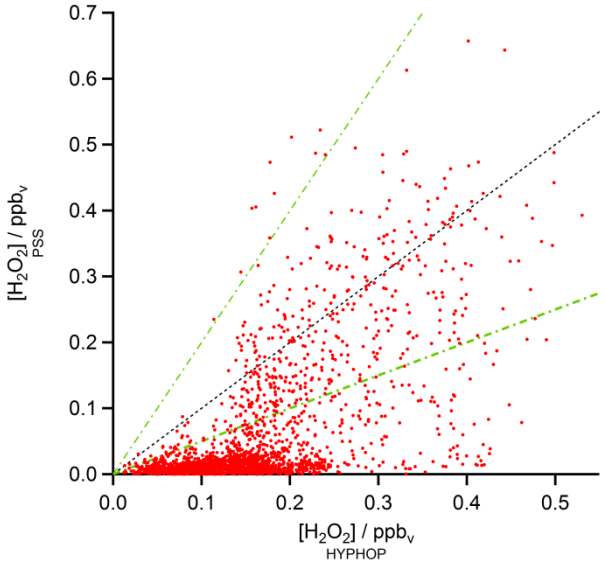

Figure 13: Scatter plot of *in situ* and PSS calculated H_2O_2 mixing ratios (red) with the 1:1 (black), 1:2 and 2:1 (both green) lines.

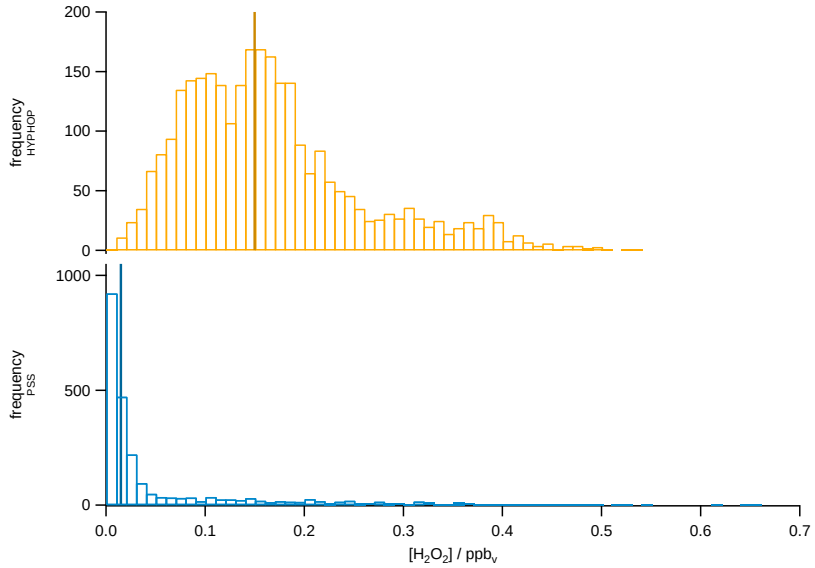

Figure 14: Histograms of *in situ* (top) and PSS (bottom) H_2O_2 mixing ratios (bars) and the associated medians (lines).

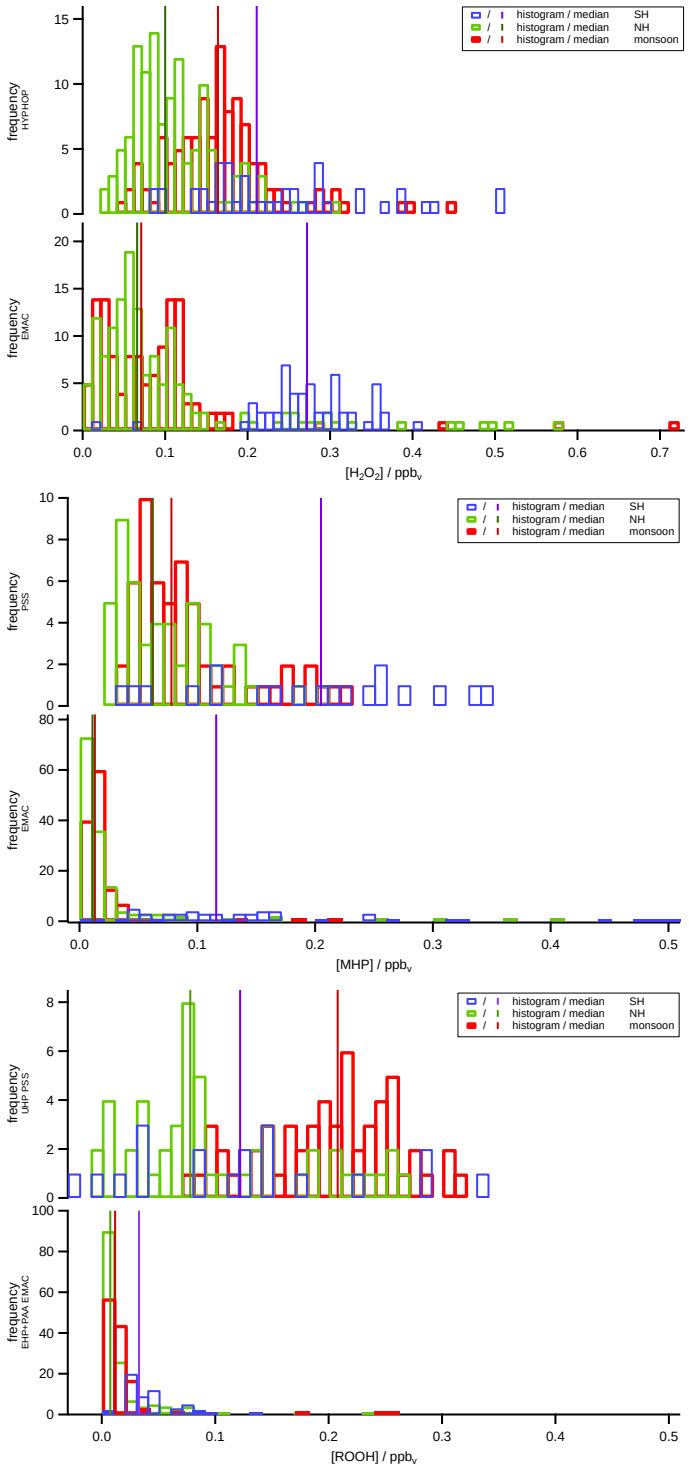

Figure 15: Histograms of *in situ* and EMAC H_2O_2 (top), PSS and EMAC-MHP (middle) and PSS and EMAC-UHP (bottom) mixing ratios during the OMO campaign for NH background (green), SH (blue) and AMA (red) air masses.

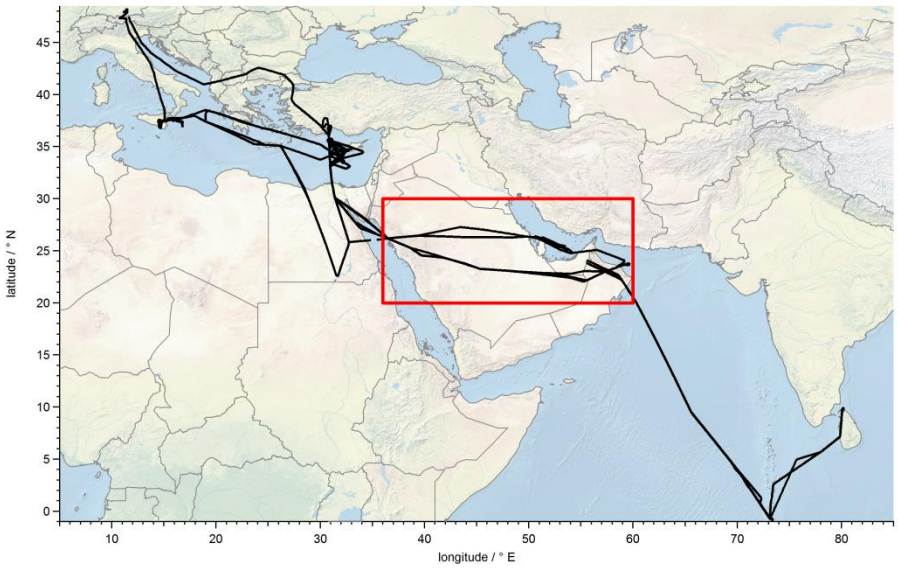

Figure 16: Location of measurements used for the longitudinal gradient study (red box) out of all flight tracks (black).

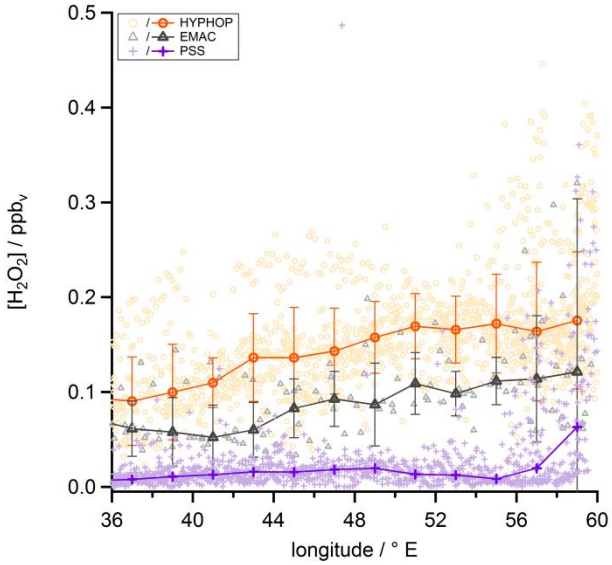

Figure 17: Longitudinal trends of *in situ* H_2O_2 mixing ratios (orange circles), EMAC-H_2O_2 (black triangles) and PSS H_2O_2 (purple crosses). The data are shown in the light colors while the darker ones represent the medians.

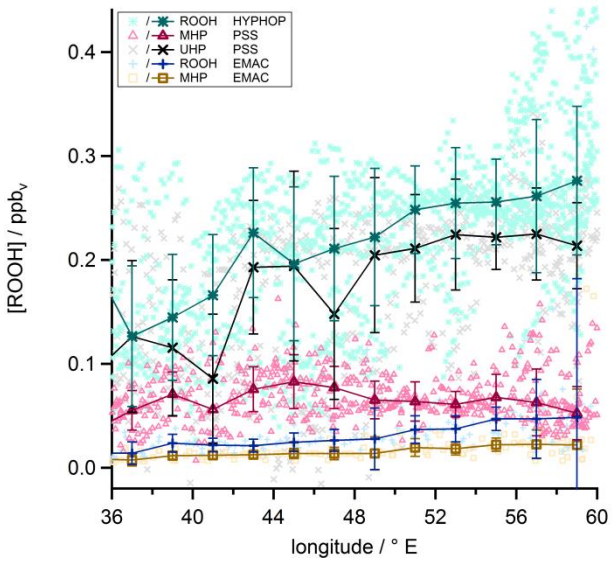

Figure 18: Longitudinal trends of in situ ROOH mixing ratios (green asterisks), EMAC-ROOH (blue plus signs) and PSS mixing ratios for MHP (pink triangles) and UHP (black crosses) as well as EMAC-MHP (yellow squares). The data are shown in the light colors while the darker ones represent the medians.

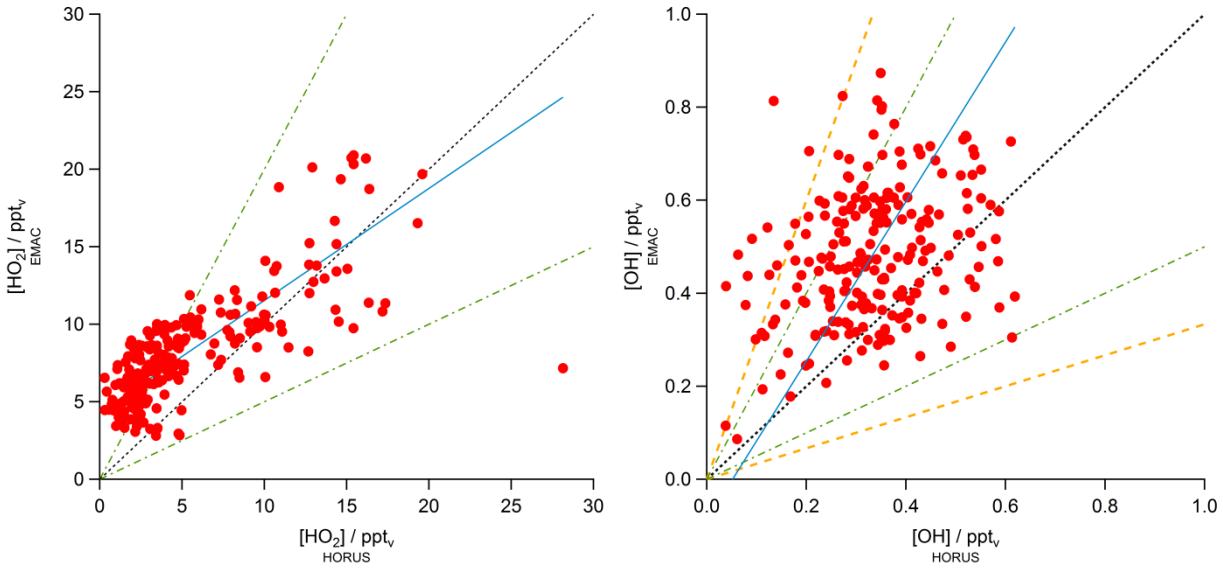

Figure 19: Scatter plot of *in situ* and EMAC HO_2 data (left) and the OH data (right) (both red) with the 1:1 (black), 1:2 and 2:1 (both green) lines. The blue line shows the calculated least orthogonal distance fit.

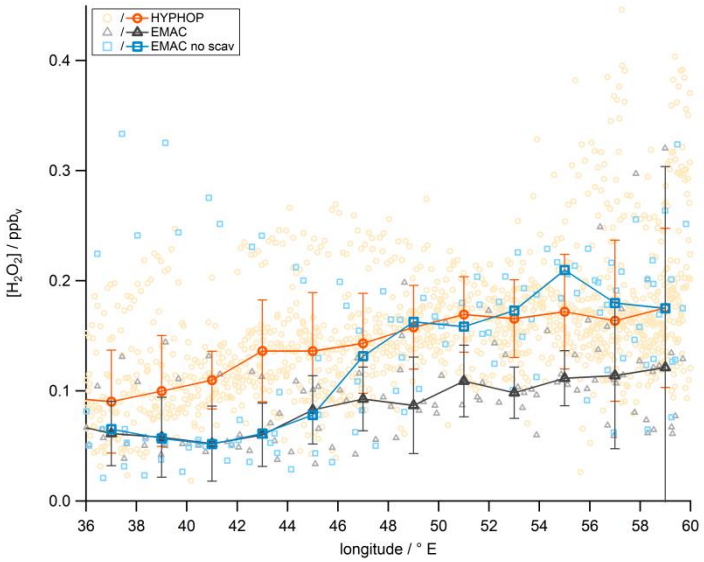

Figure 20: Longitudinal trends of in situ H_2O_2 mixing ratios (orange circles), EMAC (black triangles) and the sensitivity study without scavenging in EMAC (blue circles). The data are shown in the light colors while the darker ones represent the medians.

Table 1: Comparison of H_2O_2 mixing ratios in the upper troposphere from measurements and PSS calculations.

region	median	$[H_2O_2]/ppt_v$
PSS	median range avg±sdev	15 LOD–657 61±101
HYPHOP	median range avg±sdev	150 LOD–530 165±91

Table 2: Comparison of H_2O_2, MHP and UHP mixing ratios in the upper troposphere from EMAC, measurements and PSS calculations.

region	median	$[H_2O_2]/ppt_v$		$[MHP]/ppt_v$		$[UHP]/ppt_v$	
		EMAC	HYPHOP	EMAC	PSS	EMAC	PSS
NH background	median range avg±sdev	66 6–576 102±110	100 20–301 110±53	11 2–408 28±58	64 21–202 75±42	8 1–238 18±31	78 LOD–261 103±77
monsoon	median range avg±sdev	71 8–714 84±92	164 46–446 167±69	13 2–216 18±28	70 37–220 92±49	12 1–259 18±34	208 80–311 199±59
SH background	median range avg±sdev	272 15–409 272±68	211 85–510 238±105	116 2–502 155±125	152 40–346 191±95	33 1–132 42±24	122 LOD–334 125±102